Mature miR-17-5p and passenger miR-17-3p induce hepatocellular carcinoma by targeting PTEN, GalNT7 and vimentin in different signal pathways

Sze Wan Shan[1,2], Ling Fang[1,2], Tatiana Shatseva[1,2], Zina Jeyapalan Rutnam[1,2], Xiangling Yang[1,2], William W. Du[1,2], Wei-Yang Lu[3], Jim W. Xuan[4], Zhaoqun Deng[1,2] and Burton B. Yang[1,2,*]

[1]Sunnybrook Research Institute, Sunnybrook Health Sciences Centre, Toronto M4N 3M5, Canada
[2]Department of Laboratory Medicine and Pathobiology, University of Toronto M5S 1A8, Canada
[3]Department of Physiology and Pharmacology, Western University, London, Ontario N6A 5C1, Canada
[4]Lawson Health Research Institute, University of Western Ontario, London, Ontario N6A 4G5, Canada
*Author for correspondence (byang@sri.utoronto.ca)

Accepted 7 January 2013
Journal of Cell Science 126, 1517–1530

doi: 10.1242/jcs.122895

Summary

To study the physiological role of a single microRNA (miRNA), we generated transgenic mice expressing the miRNA precursor miR-17 and found that the mature miR-17-5p and the passenger strand miR-17-3p were abundantly expressed. We showed that mature miR-17-5p and passenger strand miR-17-3p could synergistically induce the development of hepatocellular carcinoma. The mature miR-17-5p exerted this function by repressing the expression of PTEN. In contrast, the passenger strand miR-17-3p repressed expression of vimentin, an intermediate filament with the ability to modulate metabolism, and GalNT7, an enzyme that regulates metabolism of liver toxin galactosamine. Hepatocellular carcinoma cells, HepG2, transfected with miR-17 formed larger tumors with more blood vessels and less tumor cell death than mock-treated cells. Expression of miR-17 precursor modulated HepG2 proliferation, migration, survival, morphogenesis and colony formation and inhibited endothelial tube formation. Silencing of PTEN, vimentin or GalNT7 with their respective siRNAs enhanced proliferation and migration. Re-expressing these molecules reversed their roles in proliferation, migration and tumorigenesis. Further experiments indicated that these three molecules do not interact with each other, but appear to function in different signaling pathways. Our results demonstrated that a mature miRNA can function synergistically with its passenger strand leading to the same phenotype but by regulating different targets located in different signaling pathways. We anticipate that our assay will serve as a helpful model for studying miRNA regulation.

Key words: MicroRNA, Pten, GalNT7, Vimentin, Hepatocellular carcinoma

Introduction

MicroRNAs (MiRNAs) are short strands of RNAs, 18–24 nucleotides in length. Most miRNAs bind and target the 3′-untranslated region (3′UTR) of mRNAs with imperfect complementarity and function as translational repressors. Conversely, it has been demonstrated that the 3′UTR and other non-coding RNAs can regulate miRNA functions (Jeyapalan et al., 2011; Lee et al., 2009; Lee et al., 2011). This newly discovered class of regulatory molecules has been demonstrated to exert diverse biological functions in regulating cell activities such as cell proliferation (Shatseva et al., 2011; Viticchiè et al., 2011; Yu et al., 2012), cell differentiation (Goljanek-Whysall et al., 2012; Guo et al., 2012; Kahai et al., 2009), apoptosis (Ye et al., 2011), morphogenesis (Wang et al., 2008a), invasion (Deng et al., 2011; Luo et al., 2012), tissue growth (Shan et al., 2009), tumor formation (Nohata et al., 2012; Volinia et al., 2006), angiogenesis (Lee et al., 2007; Smits et al., 2010; Zou et al., 2012), and metastasis (Huang et al., 2008; Ma et al., 2007; Rutnam and Yang, 2012a). The most intensively studied miRNAs are those involved in cancer development. Among these miRNAs, some have been reported to function as oncogenic miRNAs, while the others have been shown to serve as tumor suppressors.

After being transcribed from the genomic DNA, a primary miRNA transcript usually consists of a miRNA cluster that gives rise to multiple precursors, followed by further processing to produce mature miRNA (Altuvia et al., 2005). One of the most well studied miRNA clusters is miR-17∼92 which has paralogs miR-106b∼25 and miR-106a∼363. Several miRNAs in these clusters have been reported to play important roles in cancer development through the repression of tumor-associated genes (Bonauer and Dimmeler, 2009; Fang et al., 2012; Sylvestre et al., 2007). The oncogenic functions of miR-17∼92, miR-106b∼25, and miR-106a∼363 have been extensively reported (Dang, 2009; Fang et al., 2011; Landais et al., 2007; Matsubara et al., 2007). Overexpression of the miR-17∼92 cluster enhanced cell proliferation and reduced apoptosis by regulating cell-cycle progression (Hayashita et al., 2005; Matsubara et al., 2007; Mendell, 2005).

Biogenesis of miRNAs is a complex mechanism that involves ribonuclease III type enzymes, which cleaves long double-stranded RNA molecules (Denli et al., 2004). Initially, miRNAs are produced from primary RNA polymerase II transcripts by sequential processing within the nucleus, followed by the cytoplasm (Lee et al., 2003). Nuclear precursor RNAs are

cleaved by the endonuclease Drosha to release pre-miRNAs, which are 60–70 nucleotide-long imperfect hairpin structures (Lee et al., 2003). After being transported to the cytoplasm by exportin-5, pre-miRNAs are processed by the endonuclease Dicer, producing a mature miRNA and a passenger strand (Kiriakidou et al., 2007). The mature miRNA is the guide strand for regulation of gene expression, while the passenger strand is believed to be degraded and inactivated (Guo and Lu, 2010; Matranga et al., 2005).

We have recently found that transgenic mice expressing miR-17 precursor produce comparable levels of mature miR-17-5p and passenger miR-17-3p (Shan et al., 2009). Wang and colleagues showed that miR-17-5p and miR-17-3p are differentially expressed (Wang et al., 2008b). When adipocyte differentiation was induced, miR-17-5p expression levels were higher than those of miR-17-3p at early time points but the opposite trend was observed at later time points. This miRNA is a member of the miR-17∼92 cluster which expresses six miRNA precursors and plays important roles in gene regulation (O'Donnell et al., 2005; Xiao et al., 2008).

Results

Development of liver tumors in miR-17 transgenic mice

We have established a mouse line expressing miR-17 (Shan et al., 2009). To examine whether or not expression of miR-17 affected mature and aging tissue function, we examined organs from both wild-type (WT) and transgenic (Tg) mice and detected many liver tumors within the miR-17 transgenic mice (Fig. 1A, and supplementary material Table S1) but almost none in the wild-type C57BL/6xCBA mice (Fig. 1B). Histological examination revealed a common trabecular pattern in the tumor sections of Tg mice (Fig. 1C). Since this was an indication of hepatocellular carcinoma (HCC), we examined tumor sections in greater detail and observed a trabecular pattern, mitotic nuclei phenotype, and the presence of deformed nuclei of various sizes, all characteristic of HCC (Fig. 1D).

The Tg tumors were analyzed for HCC marker expression including AFP, CD34, GPC3, Ki67 and p53. All were shown to be present in the Tg tumors (Fig. 1E; supplementary material Fig. S1), except for p53, which was present in slightly more than half of the Tg tumors. The expression pattern of these five markers was similar to those found in HCC patient samples. It is known that ∼50% of HCC patients are p53 positive. Interestingly, CD34 was not detected in the fatty livers with severe phenotype, but could only be detected when tumors were developed (Fig. 1F).

miR-17 promotes tumorigenesis and angiogenesis by modulating various cell activities

We tested the role of miR-17 in liver tumorigenesis and angiogenesis. HepG2 cells stably transfected with miR-17 and mock were injected subcutaneously into nude mice. Eighty-nine days after injection, miR-17-transfected cells formed significantly larger tumors than mice injected with mock-transfected cells (Fig. 2A). The tumor formation assay was repeated using the same conditions and similar results were obtained. In the tumor sections derived from mock-transfected cells, we observed cells with condensed and fragmented blue nuclei after H&E staining (Fig. 2B), characteristic of dead cells. However, fewer such cells were found in the tumors formed by the miR-17 cells. The miR-17 tumors also had significantly more blood vessels than the control tumors as observed by probing with an anti-CD34 antibody (Fig. 2C; supplementary material Fig. S2A,B), implying that miR-17 was involved in angiogenesis. This was consistent with our finding that the tumors developed in the Tg mice were highly vascularized. The tumor sections were also subjected to E-cadherin and TUNEL staining to confirm cell apoptosis. More apoptotic cells were detected in the control tumors than in miR-17 tumors (Fig. 2D).

To test the effect of miR-17 on endothelial cell activities, we performed tube formation assays. The miR-17- or mock-transfected cells were mixed with YPEN cells and cultured in Matrigel. In the presence of the miR-17-transfected cells, YPEN cells formed larger complexes and longer tube-like structures compared with the control cells (supplementary material Fig. S2C), suggesting a role of miR-17 in supporting endothelial cell activity. To examine the role of miR-17 in liver cell activities, we stably expressed the miR-17 construct in HepG2 cells. Expression of mature miR-17-5p and miR-17-3p was upregulated in the miR-17-transfected cells compared with the control cells (Fig. 3A). Analysis of the levels of both strands in a number of cell lines also showed comparable levels of miR-17-5p and miR-17-3p (Fig. 3B). Although miR-17 has been found to be upregulated in HCC (Connolly et al., 2008), the functional mechanisms of this miRNA is still poorly understood. We analyzed the effect of miR-17 on HepG2 cell activities. The miR-17 cells showed an elongated cell morphology (supplementary material Fig. S2D) and cytoskeletal structure (supplementary material Fig. S2E).

Next, both mock- and miR-17-transfected HepG2 cells were seeded in soft agarose for 15 days. MiR-17-transfected cells formed larger colonies than the mock-transfected cells (supplementary material Fig. S2F). A significant increase in the number of colonies was detected in the miR-17-transfected cells compared with the control cells (Fig. 3C). In cell proliferation assays, we observed that overexpression of miR-17 led to faster cell proliferation relative to the control (Fig. 3D; supplementary material Fig. S2G). In survival assays, cells were maintained in serum-free conditions and allowed to overgrow, resulting in extensive cell death. Expression of miR-17 promoted cell survival compared with the control (Fig. 3E; supplementary material Fig. S2H). Wound healing experiments showed that the miR-17-transfected cells migrated into the wounded areas faster than the mock-transfected cells (supplementary material Fig. S3A).

To confirm the function of miR-17, both mock- and miR-17-transfected HepG2 cells were transiently transfected with a construct expressing an antisense sequence against miR-17-5p. Transfection with inhibitors decreased levels of miR-17-5p and miR-17-3p, respectively (supplementary material Fig. S3B). Examination of cell proliferation on days 1, 4 and 6 revealed that the antisense did not produce a significant effect on the control cells, but suppressed the growth of the miR-17-cells (Fig. 3F), suggesting a major role of miR-17 in cell proliferation. This could be due to a limited effect of endogenous miR-17-5p and miR-17-3p on cell proliferation.

We tested the effects of miR-17 on two different liver tumor cell lines JHH1 and SNU-449 (from ATCC). Stable expression of miR-17 promoted proliferation of JHH1 and SNU449 cells (supplementary material Fig. S3C). In tumor formation assays, only JHH1 cells were able to form tumors in nude mice. Expression of miR-17 enhanced tumor growth (supplementary material Fig. S3D). Increased levels of both miR-17-5p and miR-17-3p were confirmed by real-time PCR (supplementary material

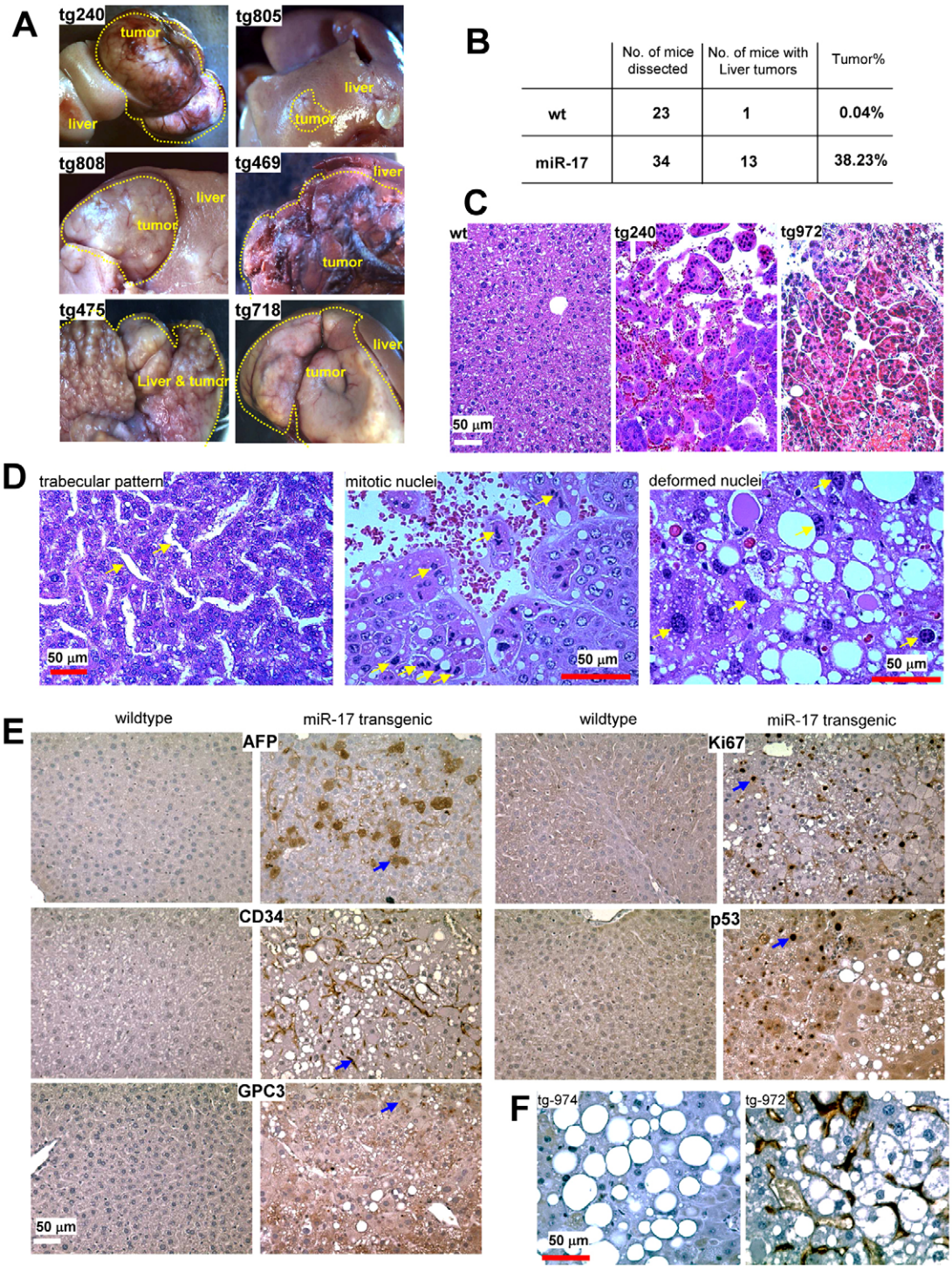

	No. of mice dissected	No. of mice with Liver tumors	Tumor%
wt	23	1	0.04%
miR-17	34	13	38.23%

Fig. 1. Expression of miR-17 induces development of liver tumors and angiogenesis. (**A**) Example of liver tumors in miR-17 transgenic mice. (**B**) Liver tumors developed extensively in miR-17 transgenic mice. (**C**) H&E staining indicated presence of HCC in the miR-17 mice. (**D**) The H&E-stained liver tumors were examined in detail for trabecular pattern, mitotic nuclei (pattern/shape/numbers), and for the presence of deformed nuclei of different sizes, all of which are characteristics of HCC (examples indicated by yellow arrows). (**E**) The wild-type and Tg liver sections were probed for five markers of HCC (as indicated). Expression of these markers was detected in Tg liver tumor sections but not in the wild-type sections (blue arrows). (**F**) Expression of CD34 was detected only in liver tumors (tg972) but not in the fatty liver (tg974). Scale bars: 50 μm.

Fig. S3E). Immunohistochemistry analysis indicated that the miR-17 tumors expressed higher and stronger CD34 levels than the control tumors (supplementary material Fig. S3F). Examination of the tumor sections after H&E staining revealed extensive cell death in the control tumors but not in the miR-17 tumors (supplementary material Fig. S3G), which was confirmed

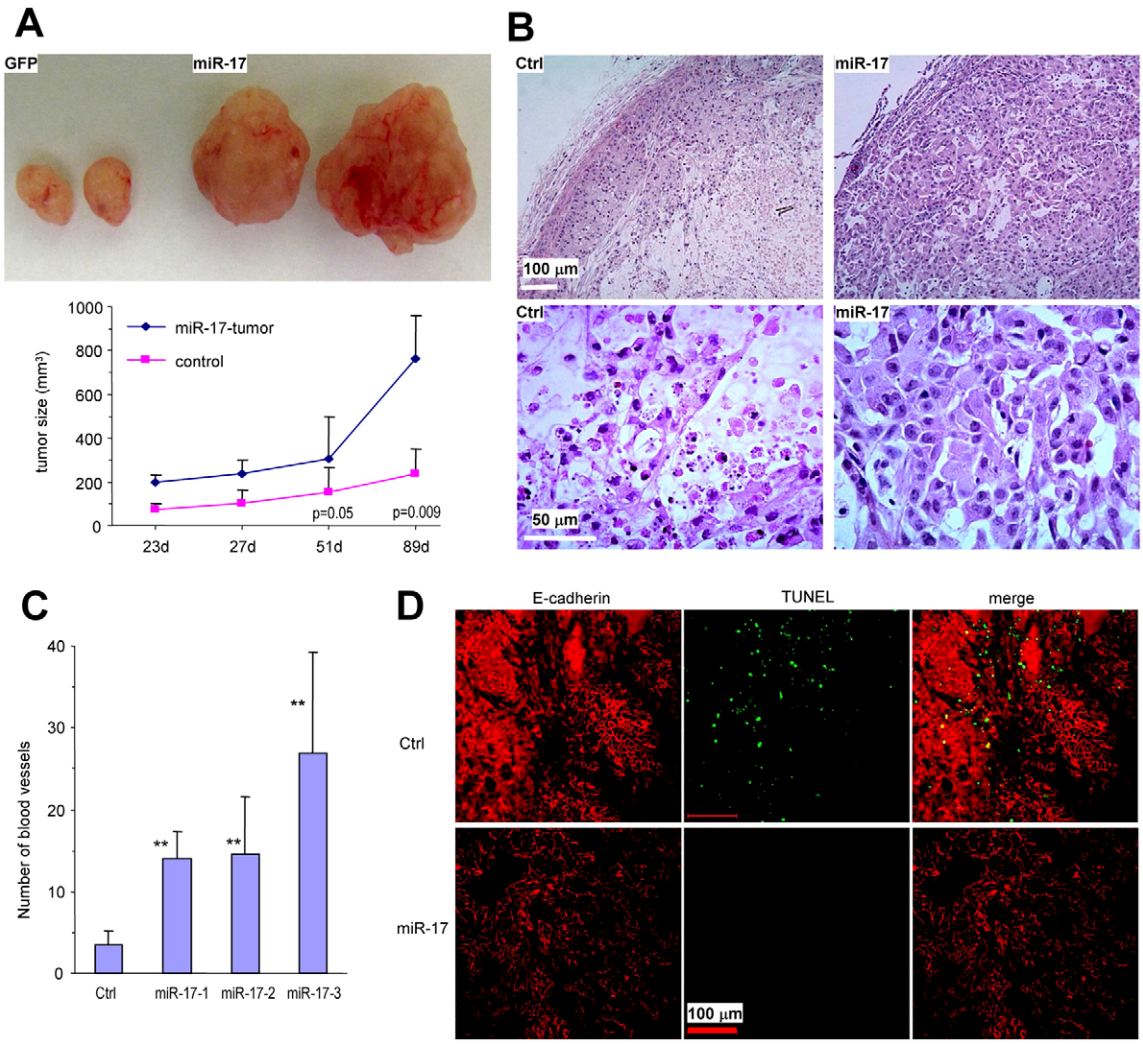

Fig. 2. Tumor formation and angiogenesis affected by miR-17 expression. (**A**) miR-17- or mock-transfected HepG2 cells were injected into nude mice. Ninety days after injection, mice were sacrificed. Tumors were removed and photographed (Top). Tumor sizes were measured (Bottom). Error bars indicate the s.d. (n=5). (**B**) H&E staining of tumor sections showed more dead cells in the control tumors than in the miR-17 tumors. (**C**) The number of blood vessels in each tumor type were counted. $^{**}P<0.01$. Error bars indicate the s.d. (**D**) Apoptotic cells in the tumor sections were analyzed by TUNEL. Immunostaining with anti-E-cadherin antibody was used for background staining. Expression of miR-17 reduced tumor cell death.

by TUNEL staining for quantification (supplementary material Fig. S3H).

Expression of PTEN, Vimentin and GalNT7 is repressed

Computational algorithm indicated that the miR-17 precursor could produce a mature miR-17-5p and a passenger miR-17-3p strand (http://www.mirbase.org/cgi-bin/mirna_entry.pl?acc=MI0000071), which share no significant homology in their seed regions (supplementary material Fig. S4A). We previously detected that the young Tg mice expressed both miR-17-5p and miR-17-3p at comparable levels (Shan et al., 2009). Here we examined both strands in the aging mice and found that both miR-17-5p and miR-17-3p were upregulated in the livers (supplementary material Fig. S4B) as well as in other organs (supplementary material Fig. S4C). Expression of miR-17-5p was detected in livers at different time points (supplementary material Fig. S4D). Direct evidence of the presence of miR-17-3p was provided by northern blotting (supplementary material Fig. S4E). To support this observation, we expressed miR-17 in a number of cell lines including HepG2 (supplementary material Fig. S4F), PC3, Hek293, and U87 (data not shown) and found that miR-17-5p and miR-17-3p were equally expressed.

It has been reported that cells expressing miR-17~92 express lower levels of phosphatase and tensin homolog deleted on chromosome 10 (PTEN) (Xiao et al., 2008), but it is not known which miRNA is responsible for the PTEN repression. PTEN deletion in mice hepatocytes developed phenotypes similar to those in HCC (Horie et al., 2004). We analyzed PTEN levels and found that expression of PTEN was greatly repressed in the miR-17 mice compared with WT mice (Fig. 4A; supplementary material Fig. S5A). To confirm this, we transiently transfected HepG2 cells with miR-17 and detected decreased levels of PTEN compared with mock-transfected cells (Fig. 4A). Furthermore, HepG2 cells stably transfected with miR-17 expressed lower levels of PTEN (Fig. 4A). Analysis of PTEN mRNA levels revealed a non-significant difference between both groups of

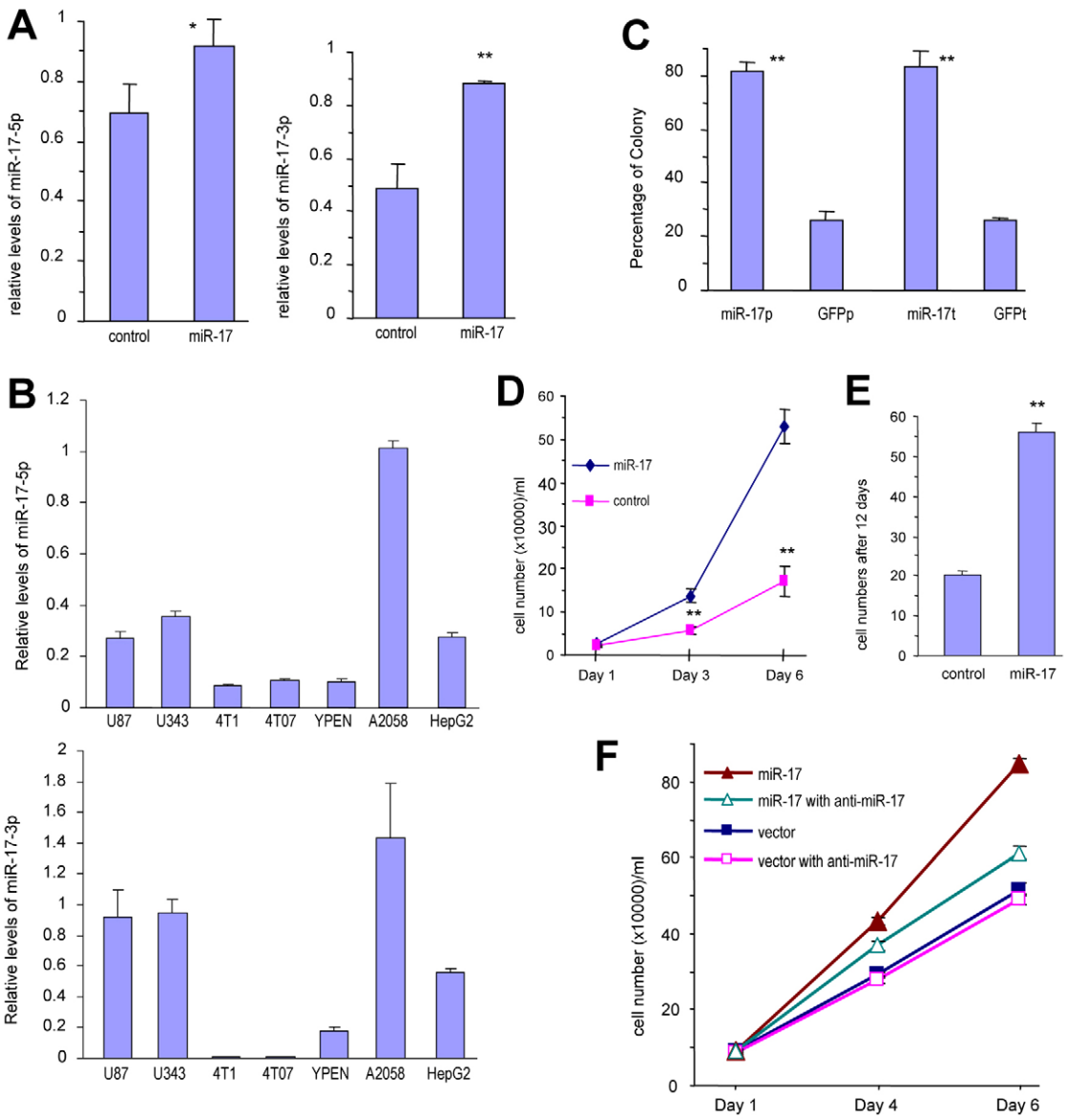

Fig. 3. Expression of miR-17 affects HepG2 cells activities. (**A**) Expression of mature miR-17-5p and miR-17-3p was analyzed by real-time PCR using RNAs isolated from miR-17- and mock-transfected HepG2 cells. Both miR-17-5p and miR-17-3p were upregulated. ($n=3$ PCRs; data are means ± s.d., $*P<0.05$, $**P<0.01$). (**B**) Expression of mature miR-17-5p and miR-17-3p were analyzed by real-time PCR using RNAs isolated from different cell lines as indicated. miR-17-5p and miR-17-3p were comparably expressed ($n=3$ PCRs; data are means ± s.d.). (**C**) Percentages of colonies formed by mock- and miR-17-transfected HepG2 cells (p), and cells isolated from GFP and miR-17 tumors (t). (**D**) The number of GFP- and miR-17-transfected cells was counted on days 1, 3 and 6 to determine proliferation rates. (**E**) miR-17- or mock-transfected cells were maintained in serum-free conditions. The surviving cells were harvested and counted. Transfection with miR-17 enhanced cell survival. (**F**) GFP- and miR-17-transfected cells were transfected transiently with miR-17-5p antisense. The cells were counted on days 1, 4 and 6 to determine growth rate. miR-17-transfected cells showed faster proliferation, but incubation with the miR-17-5p antisense abolished this effect. Asterisks indicate significant differences. Data are means ± s.d., $n=12$ trials, $*P<0.05$, $**P<0.01$.

cells (supplementary material Fig. S5B), suggesting post-transcriptional suppression of PTEN by miR-17.

We further examined PTEN repression *in vivo*. PTEN expression was greatly repressed in the miR-17 tumors (supplementary material Fig. S5C). Western blot analysis showed that PTEN expression was lower in tumors formed by injection of miR-17-transfected cells than in tumors formed by the mock-transfected cells (Fig. 4A). We further examined PTEN expression in liver tumors from both WT and Tg mice and observed a repression of PTEN expression in Tg livers relative to WT livers (supplementary material Fig. S5D). These results were consistent with the expression pattern of PTEN from HCC patient samples.

Bioinformatics analyses indicated that there were two potential miR-17-5p target sites in PTEN 3′UTR (Fig. 4B). Luciferase assays were performed to confirm targeting of PTEN by miR-17-5p. We generated two PTEN 3′UTR luciferase constructs (Luc-Pten1 and Luc-Pten2) harboring the two binding sites of miR-17-5p and two constructs in which miR-17-5p target sites were mutated (Luc-Pten-mut1 and Luc-Pten-mut2) (Fig. 4B; supplementary

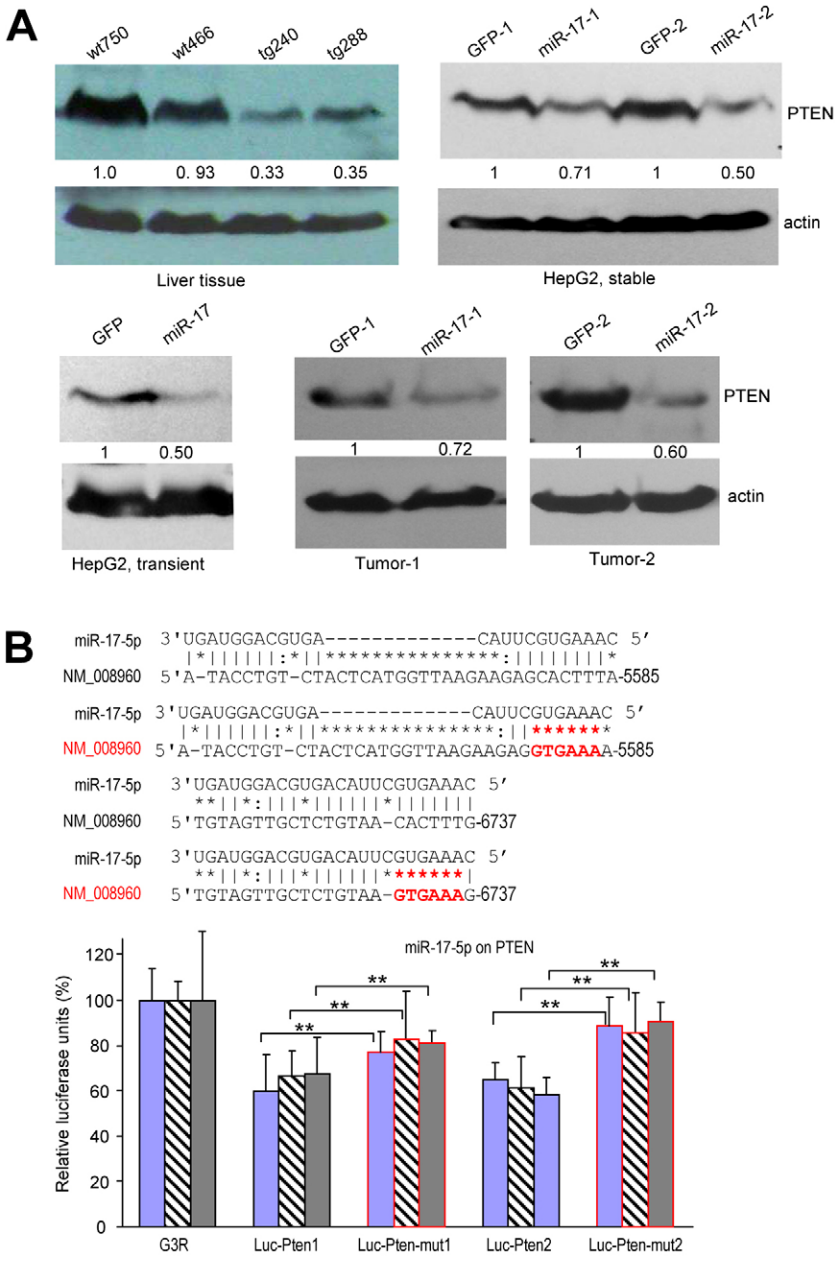

Fig. 4. PTEN as a potential target. (**A**) Protein lysates prepared from miR-17 and WT livers, from two sets of tumors (mock and miR-17), and from miR-17- or mock-transfected HepG2 cells were examined by western blotting for GalNT7 expression. Detection of β-actin on the same membranes served as a loading control. Expression of miR-17 decreased PTEN levels. (**B**) Top: structures of miR-17-5p targeting PTEN, and mutations of the target sites. Bottom: U343 cells were co-transfected with miR-17-5p mimic and a luciferase reporter construct, which was engineered with a fragment of the PTEN 3′UTR harboring the miR-17-5p target site (Luc-PTEN1 or Luc-PTEN2) or a mutant site (Luc-PTEN-mut1 or Luc-PTEN-mut2). As a negative control, the luciferase reporter vector was engineered with a non-related fragment of cDNA (G3R). Asterisks indicate significant difference. $^{**}P<0.01$. Error bars indicate the s.d. ($n=3$). The differently shaded bars show the results from three independent experiments.

material Fig. S5E). U343 cells (obtained from ATCC) were co-transfected with either PTEN 3′UTR luciferase constructs (Luc-Pten1 or Luc-Pten2) or mutant constructs (Luc-Pten-mut1 or Luc-Pten-mut2), along with miR-17-5p oligos. Significant repression of luciferase activity was detected in both sets of Luc-Pten-transfected cells, while mutation of the binding sites reversed the effects of miR-17-5p on this repression (Fig. 4B).

It has been reported that passenger miRNA strands are expressed at lower levels than their counterpart strand. Our results from *in vivo* and *in vitro* experiments indicated that the levels of miR-17-3p were, in fact, higher than that of miR-17-5p. Two questions were raised: whether miR-17-3p plays a role in the system of our studies and whether miR-17-3p could function synergistically with miR-17-5p, contributing to the phenotypes observed. Bioinformatics analyses indicated that miR-17-3p potentially targeted many mRNAs. We focused on those that were known to be important in cell metabolism, cell differentiation, and liver tumorigenesis. After extensive analysis with western blotting, we found that vimentin (GenBank accession no. NM_011701.4) and GalNT7 (NM_00116798.1) were of potential interest.

GalNT7 is an enzyme involved in the glycosylation of proteins (Kahai et al., 2009), with a putative role in the initiation of O-glycosylation (Geary et al., 2009). We found that GalNT7 expression was significantly lower in Tg liver lysates than in WT livers (Fig. 5A). Repression of GalNT7 expression was found to be associated with the tumor area in the Tg liver (supplementary material Fig. S6A). To confirm the association of GalNT7 inhibition with tumor formation, we analyzed GalNT7 levels in the HepG2 cells stably transfected with miR-17 or mock and observed repression of GalNT7 in the miR-17-cells (Fig. 5A). Tumors formed by these cells in nude mice were also analyzed

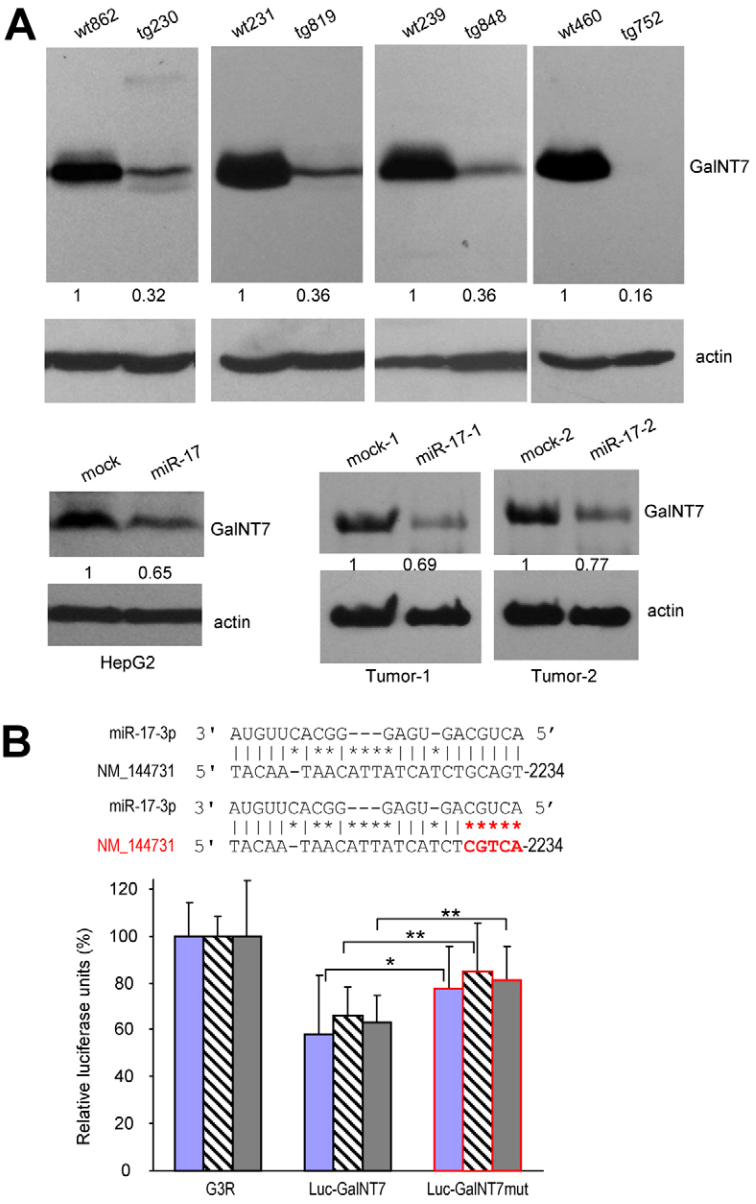

Fig. 5. GalNT7 as a potential target. (**A**) Protein lysates prepared from miR-17 and WT livers, from two sets of tumors (mock and miR-17) and from miR-17- or mock-transfected HepG2 cells were examined by western blotting for PTEN expression. Expression of miR-17 decreased PTEN levels. (**B**) Top: structures of miR-17-3p targeting GalNT7 and mutation of the target site. Bottom: Luciferase activity assays using a fragment of the GalNT7 3′UTR indicated that miR-17-3p repressed luciferase activities when it harbored GalNT7 3′UTR. The effects were abolished when the potential miR-17-3p target sites were mutated ($n=3$, $^{*}P<0.05$, $^{**}P<0.01$). The differently shaded bars show the results from three independent experiments.

for GalNT7 expression. A clear-cut repression of GalNT7 in the miR-17 tumors compared with mock tumors was detected by western blotting (Fig. 5A) and by immunohistochemistry (supplementary material Fig. S6B), but not at the mRNA level (supplementary material Fig. S6C).

To further confirm that GalNT7 was a target of miR-17-3p, we generated a luciferase construct harboring a fragment of the GalNT7 3′UTR containing the miR-17-3p target sequence (Luc-GalNT7) (supplementary material Fig. S5E). A mutant construct (Luc-GalNT7-mut) was also made (supplementary material Fig. S5E) by mutating the seed region targeted by miR-17-3p (Fig. 5B). In three separate experiments, luciferase activity was significantly repressed when Luc-GalNT7 was co-transfected with miR-17 (Fig. 5B). Mutation of the miR-17-3p target site abolished the effects of miR-17-3p, suggesting that miR-17-3p could repress GalNT7 expression by binding to GalNT7 3′UTR. Sequence analysis indicated that the miR-17-3p target sequence was highly conserved across different species (supplementary material Fig. S6D).

Vimentin is another potential target of miR-17-3p. The miR-17-3p target site of vimentin 3′UTR has also been shown to be highly conserved across different species (supplementary material Fig. S6E), suggesting a physiological role of this sequence. Vimentin is a cytoplasmic intermediate filament (cIF) which is widely distributed in most cell types (Klymkowsky et al., 1989). Cells lacking vimentin are unable to transport low-density lipoprotein (LDL)-derived cholesterol from their lysosomes to the endoplasmic reticulum for esterification (Sarria et al., 1992). It has also been reported that increased levels of cholesterol synthesis was detected in cells lacking a cIF network (Sarria et al., 1992).

Using similar approaches, we examined vimentin expression in the miR-17 livers, miR-17-transfected HepG2 cells, and miR-17 tumors. In all these tests, we detected a repression of vimentin

levels (Fig. 6A). We further examined vimentin levels in other tissues including heart, skin and lung. Vimentin expression was downregulated in the miR-17 transgenic heart and skin compared with the WT tissues (supplementary material Fig. S6F). Immunohistochemical analysis of vimentin expression in the miR-17 livers showed that repression of vimentin expression was clearly seen in the liver tumors of the miR-17 mice (supplementary material Fig. S6G). This was supported by immunohistochemistry of miR-17 and mock tumors, in which we observed that the miR-17 tumors, which were significantly larger in size, expressed much lower levels of vimentin than the mock tumors (supplementary material Fig. S6H). We also confirmed that the miR-17 tumors derived from JHH-1 cells expressed lower levels of PTEN, GalNT7 and vimentin than the GFP tumors (supplementary material Fig. S7A).

To further establish vimentin as a target of miR-17-3p, we generated luciferase constructs harboring the vimentin 3′UTR (Luc-Vim) or mutated 3′UTR (Luc-Vim-mut1 and Luc-Vim-mut2) (supplementary material Fig. S5E). U343 cells were transiently transfected with Vim-3′UTR constructs or the mutated constructs along with miR-17-3p oligos. Co-transfection with miR-17-3p reduced luciferase activity of Luc-Vim significantly, but not the activities of Luc-Vim-mut1 and Luc-Vim-mut2 (Fig. 6B). Thus, we confirmed the effect of endogenous miR-17-5p and miR-17-3p by transiently transfecting HepG2 cells with these luciferase constructs. To confirm the effects of endogenous miR-17, we transfected HepG2 cells with Luc-PTEN1, Luc-PTEN2, Luc-GalNT7 and Luc-VIM constructs, all of which led to lower levels of luciferase activities than transfection with the control construct G3R (supplementary material Fig. S7B). Mutation of the target sites abolished the effect of endogenous miR-17-5p and miR-17-3p.

Confirmation of miR-17-5p/miR-17-3p targeting

To confirm the targeting results, we transfected HepG2 cells with miR-17-5p and miR-17-3p inhibitors. We found that transfection with the miR-17-5p inhibitor enhanced PTEN expression, while transfection with the miR-17-3p inhibitor increased GalNT7 and

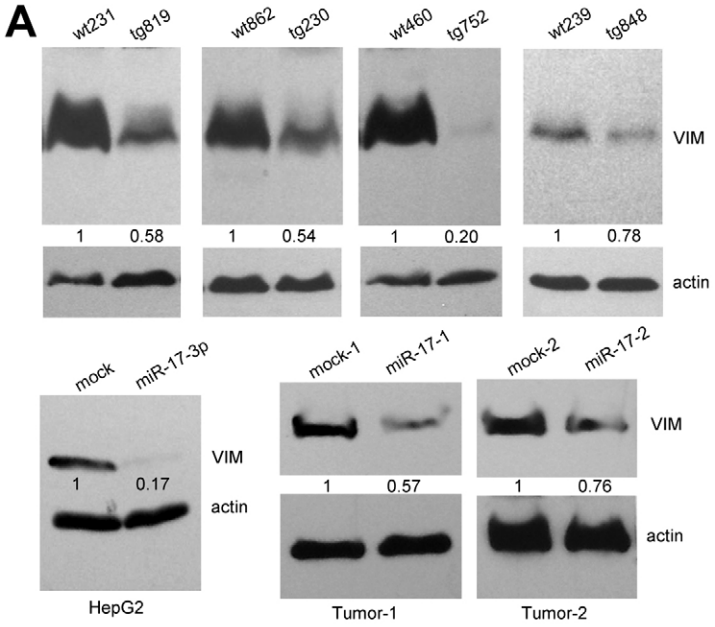

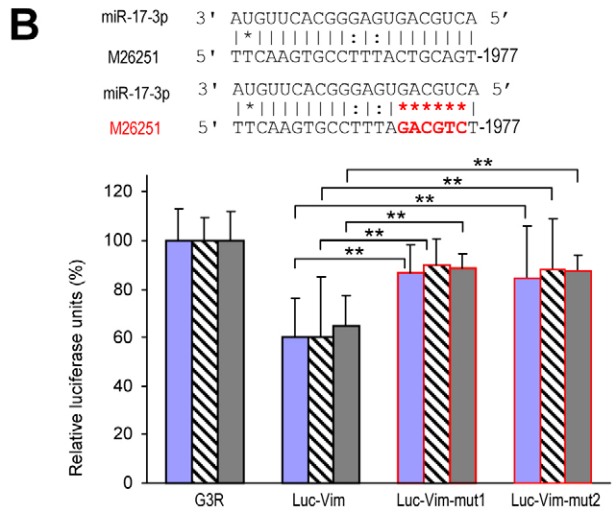

Fig. 6. Vimentin as a potential target. (**A**) Protein lysates prepared from miR-17 and WT livers, from two sets of tumors (mock and miR-17) and from miR-17- or mock-transfected HepG2 cells were examined by western blotting for vimentin expression. Expression of miR-17 decreased vimentin levels. (**B**) Top: structures of miR-17-3p targeting vimentin and mutation of the target site. Bottom: Luciferase activity assays using a fragment of vimentin 3′UTR indicated that miR-17-3p repressed luciferase activities when it harbored vimentin 3′UTR. The effects were abolished when the potential miR-17-3p target sites were mutated ($n=3$, $^{*}P<0.05$, $^{**}P<0.01$). The differently shaded bars show the results from three independent experiments.

vimentin levels (Fig. 7A). This result demonstrated that both endogenous miR-17-5p and miR17-3p could contribute to the development of HCC.

To corroborate the results, small interfering RNAs (siRNA) complementary to PTEN, GalNT7 and vimentin were synthesized. Downregulation of PTEN, GalNT7 and vimentin were confirmed by Western blotting (supplementary material Fig. S7C). Cell proliferation assays showed that transfection with PTEN, GalNT7 or vimentin siRNA significantly enhanced HepG2 cell proliferation (Fig. 7B), suggesting that PTEN-, GalNT7- and vimentin-mediated pathways were essential for miR-17-enhanced HepG2 proliferation. To confirm the involvement of these three targets on miR-17-mediated cell migration, wound healing assays were performed on the PTEN-, GalNT7- and vimentin-silencing HepG2 cells. We detected enhanced migration in the HepG2 cells transfected with siRNA targeting PTEN, GalNT7 and vimentin compared with those transfected with control oligos (Fig. 7C). These results indicated that PTEN, GalNT7 and vimentin were highly associated with HepG2 cell migration. It also suggested that these three proteins could mediate miR-17 effects in these cells.

To further confirm that miR-17-5p/miR-17-3p targeting of PTEN, GalNT7 and vimentin could affect cell proliferation and migration, rescue experiments were performed. PTEN, GalNT7 and vimentin expression constructs were generated. HepG2 cells stably transfected with miR-17 were transiently transfected with one of the expression constructs and a control vector for proliferation and wound healing assays. Upregulation of protein expression after transfection with PTEN, GalNT7 and vimentin expression constructs was confirmed by western blotting (supplementary material Fig. S7D). Significant suppression in cell proliferation was observed in the miR-17-cells transfected with PTEN, GalNT7 or vimentin compared with controls (Fig. 8A). This further confirmed that PTEN-, GalNT7- and vimentin-mediated pathways were essential for miR-17-enhanced HepG2 cell growth.

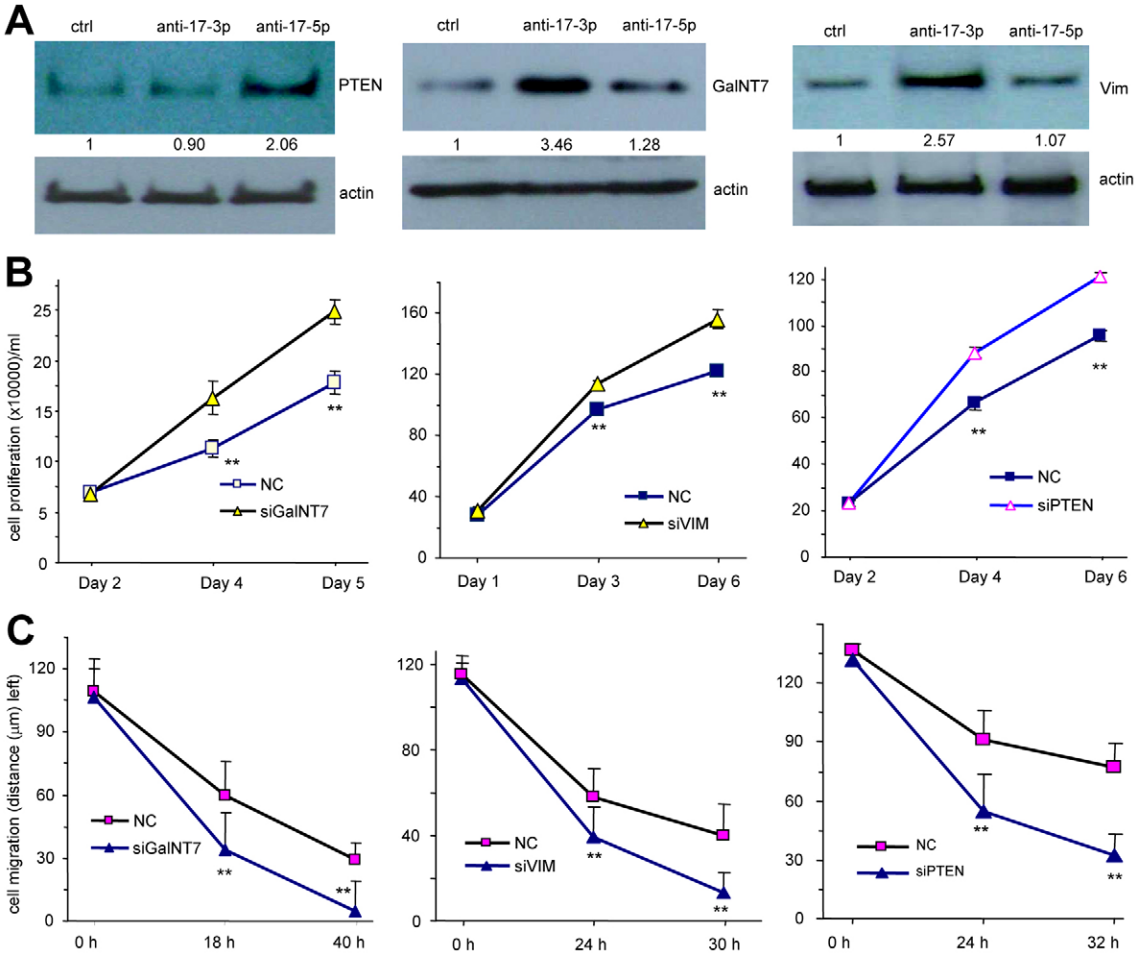

Fig. 7. Confirmation of PTEN, GalNT7 and vimentin functions using siRNA. (**A**) HepG2 cells were transfected with miR-17-5p inhibitor (anti-17-5p), miR-17-3p inhibitor (anti-17-3p), or a control oligo, followed by target analysis by western blotting. Transfection with miR-17-5p inhibitor promoted PTEN expression, whereas transfection with miR-17-3p inhibitor increased levels of GalNT7 and vimentin. (**B**) HepG2 cells were transiently transfected with PTEN-, GalNT7- and vimentin-siRNA, and then used for proliferation assays. The number of cells was counted at different time intervals to determine proliferation rates. Silencing GalNT7, vimentin, or PTEN promoted cell proliferation. Data are means ± s.d., $n=3$, $^{**}P<0.01$. (**C**) HepG2 cells were transiently transfected with PTEN-, GalNT7- or vimentin-siRNA, and were grown to sub-confluence. The monolayer of cells was scrapped for migration assays. The cells were fixed at the indicated time points. The distances between the wounded center and the front of the migrating cells (vertical axis) were measured. Silencing GalNT7, vimentin, or PTEN promoted cell migration. Data are means ± s.d., $n=30$, $^{**}P<0.01$.

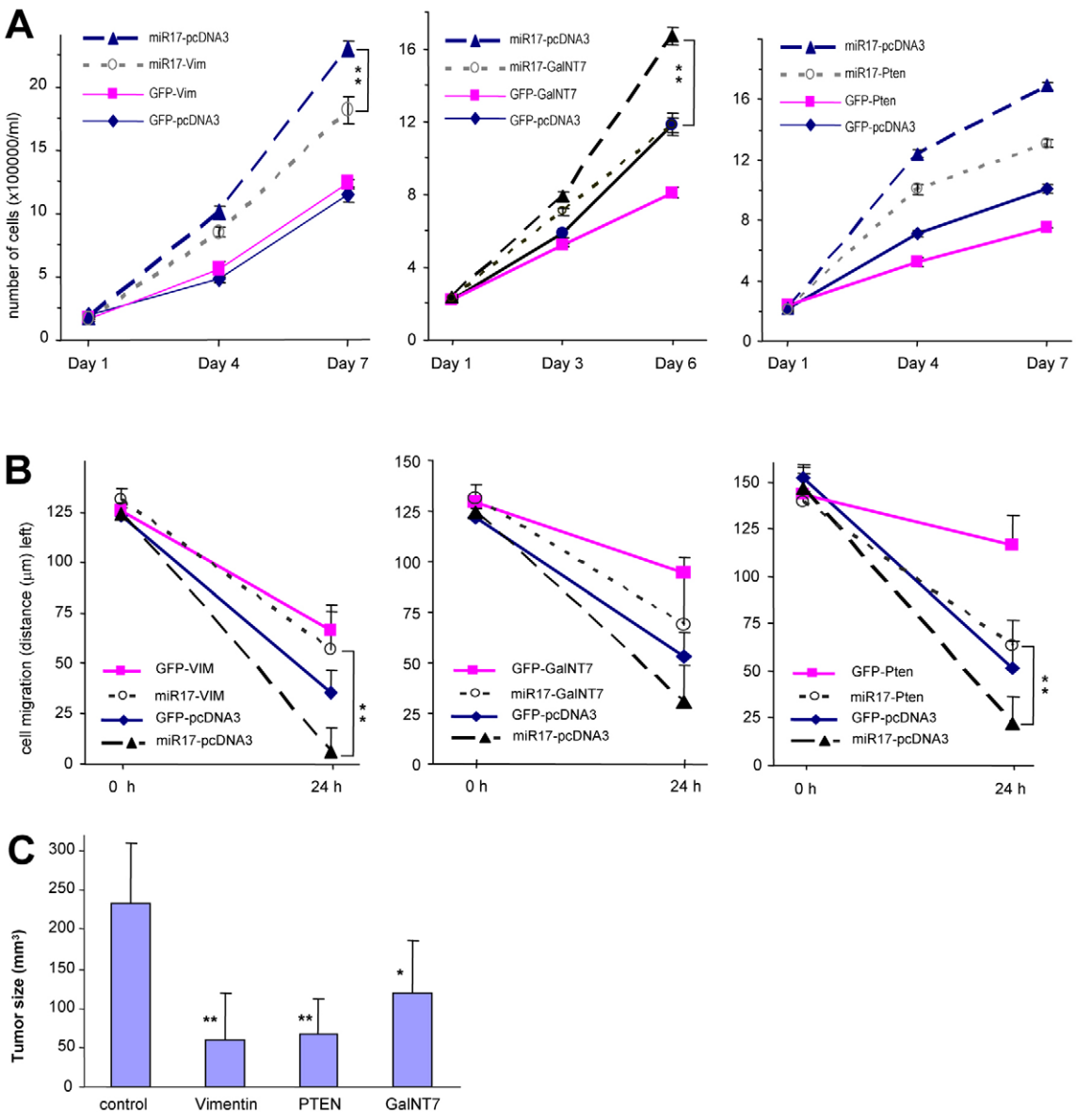

Fig. 8. Confirmation of PTEN, GalNT7 and vimentin functions by rescue assay. (**A**) HepG2 cells stably expressing miR-17 were transiently transfected with expression constructs of PTEN, GalNT7, and vimentin. The cells were cultured and cell numbers were counted on days 1, 4 and 7 to determine the rate of cell proliferation. Expression of GalNT7, vimentin, or PTEN reversed miR-17-3p or miR-17-5p function. Data are means ± s.d., $n=3$, $^{**}P<0.01$. (**B**) HepG2 cells stably expressing miR-17 were transiently transfected with PTEN, GalNT7 or vimentin. Expression of PTEN-, GalNT7- or vimentin reversed the effect of miR-17 in suppressing cell migration. Data are means ± s.d., $n=30$, $^{**}P<0.01$. (**C**) HepG2 cells transfected with miR-17 were transiently transfected with the above expression constructs, and then injected subcutaneously into nude mice. Tumor growth was monitored for up to 6 weeks. Expression of PTEN-, GalNT7- or vimentin reversed the effect of miR-17 in tumor formation. Data are means ± s.d., $n=5$, $^{*}P<0.05$, $^{**}P<0.01$.

We confirmed the involvement of PTEN, GalNT7 and vimentin on miR-17-mediated cell migration. We found that the enhanced migration of miR-17-transfected cells was abolished by overexpressing PTEN, GalNT7 or vimentin (Fig. 8B; supplementary material Fig. S8A). These results suggested that miR-17-induced activation of cell migration was largely attributable to the loss of PTEN, GalNT7 or vimentin. Reintroduction of any of these targets into the miR-17-expressing cells reversed the effect of miR-17 on cell migration and proliferation. This suggested that PTEN, GalNT7 and vimentin were involved in mediating miR-17-enhanced cell migration and proliferation.

To determine whether the effect of miR-17 on tumor formation was due to the impairment of the above target proteins, we generated three expression constructs by inserting the coding sequences of PTEN, GalNT7 and vimentin into a retroviral vector pBABE, producing pBABE-PTEN, pBABE-GalNT7 and pBABE-Vim (supplementary material Fig. S8B). The miR-17 stable HepG2 cells were transfected with these three constructs and the control vector, producing four different cell lines. The cell lines were injected subcutaneously into nude mice for tumor growth assays. The mice injected with the pBABE-transfected cells displayed much larger tumors than mice injected with the

PTEN-, GalNT7- or vimentin-transfected cells (Fig. 8C). Increased expression of these proteins was further supported by immunohistochemistry (supplementary material Fig. S8C). These results indicated that PTEN, GalNT7 and vimentin were important molecules in mediating miR-17-enhanced tumorigenesis.

MiR-17 downregulates vimentin, GalNT7 and PTEN independently

Since PTEN is a negative regulator of PI3K and Akt signaling pathway, we analyzed Akt activity in HepG2 cells stably transfected with miR-17 and in tissues from the miR-17 transgenic and wild-type mice. We confirmed that expression of miR-17 enhanced levels of pAkt in miR-17-transfected HepG2 cells, and in miR-17 transgenic hearts, lungs and livers compared with controls (Fig. 9A).

Our results above showed that PTEN, GalNT7 and vimentin could synergistically mediate miR-17-5p and miR-17-3p functions. We investigated whether there was cross-talk or any interactions between these three proteins. As mentioned previously, transfection of PTEN, GalNT7 and vimentin siRNAs repressed PTEN, GalNT7 and vimentin expression, respectively, in HepG2 cells (Fig. 9B). We examined whether vimentin and GalNT7 expressions were affected by silencing PTEN in HepG2 cells. Our experiments indicated that silencing PTEN did not affect expression of GalNT7 and vimentin (Fig. 9C), suggesting that GalNT7 and vimentin were not downstream of PTEN.

Using the same approach, we observed that downregulation of GalNT7 in HepG2 cells did not affect PTEN and vimentin expression (Fig. 9D). Finally, vimentin silencing did not affect expression of PTEN and GalNT7 (Fig. 9E). These results showed that none of the three molecules were downstream of each other. In other words, PTEN, GalNT7 and vimentin functioned independently in mediating the roles of miR-17-5p and miR-17-3p.

Discussion

Our results indicated that miR-17 induced the development of liver cancer, and these effects could partially be attributed to the mediation of PTEN and GalNT7 activity, which then functioned independently but lead to the phenotype observed. PTEN is well

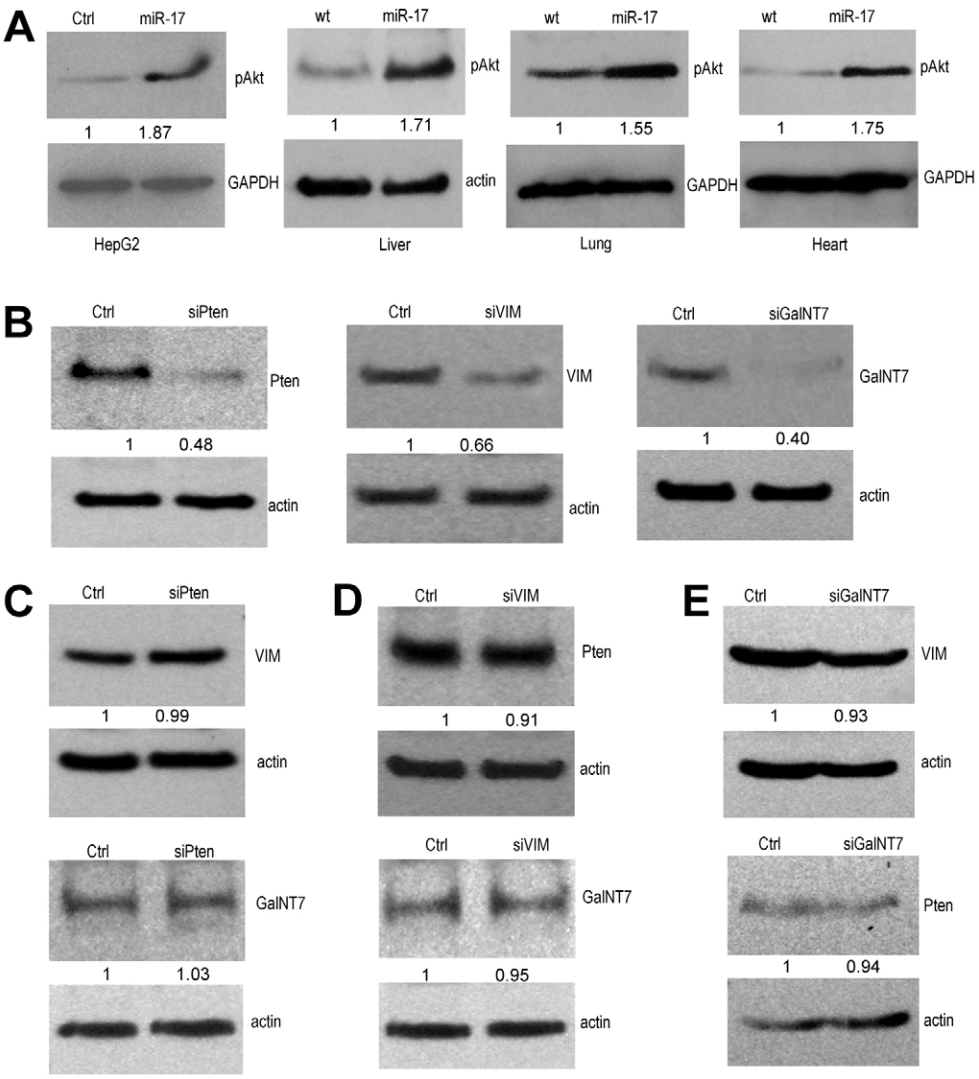

Fig. 9. MiR-17 downregulated vimentin, GalNT7 and PTEN independently. (**A**) Protein lysates prepared from HepG2 cells transfected with miR-17 or GFP and from miR-17 transgenic and wild-type liver, lung and heart were subjected to western blot analysis using anti-pAkt antibody. Upregulation of pAkt was detected in the miR-17-transfected cells and miR-17 transgenic tissues. (**B**) HepG2 cells were transfected with siRNAs against PTEN, GalNT7 or vimentin. Western blot analysis was performed to confirm silencing of these proteins. (**C**) Protein lysates prepared from HepG2 cells transfected with siRNA against PTEN were analyzed by western blotting and probed with antibodies against GalNT7 or vimentin. Little difference was detected. (**D**) Protein lysates prepared from HepG2 cells transfected with siRNA against vimentin were analyzed on western blots probed with antibodies against GalNT7 or PTEN. Little difference was detected. (**E**) Protein lysates prepared from HepG2 cells transfected with siRNA against GalNT7 were analyzed on western blots probed with antibodies against vimentin or PTEN. Little difference was detected.

studied tumor suppressor (Horie et al., 2004), while GalNT7 is a suppressor of metastasis mediating miR-30b/30d function (Gaziel-Sovran et al., 2011). Previous studies have demonstrated that expression of the miR-17-92 polycistron is upregulated in hepatocellular carcinoma patients (Connolly et al., 2008; Li et al., 2009). While expression of miR-122 is downregulated, miR-17 is upregulated in hepatocellular carcinoma patients and in rodent (Kutay et al., 2006). It was shown that miR-17 could promote migration of HCC cells (Yang et al., 2010). Our study and others suggest that miR-17 may function as an oncogenic miRNA in liver.

It is important to note that both mature miR-17-5p and the passenger strand miR-17-3p were involved. Although it is well accepted that the passenger strand of a siRNA does not play any function, the guide and passenger strands of miRNAs are not always perfectly complementary, suggesting that Dicer may not exert the same effect on a miRNA as it does to a siRNA. Dicer selects any one sequence of the hairpin structure as the guide strand and allows the rest to be degraded depending on environmental conditions. This possibility was supported by results from Wang and colleagues showing that miR-17-5p and miR-17-3p could be differentially expressed during different time point in cell culture (Wang et al., 2008b) and by our recent observation that both miR-17-5p and miR-17-3p were highly expressed in miR-17 transgenic mice. It is possible that Dicer and its associated proteins selectively generate the mature strands, the star strands or both based on the cellular needs. We have recently demonstrated that mice expressing miR-17 grew slower in the early stages of development (Shan et al., 2009). It is possible that miR-17-5p and miR-17-3p target different mRNAs in different stages of development and play varying roles in development and tumorigenesis. How these two strands of miRNA coordinate regulation of protein expression leading to phenotypic change awaits further investigation.

The important finding in our study was that the mature miR-17-5p and the passenger strand miR-17-3p could cooperatively induce hepatocellular carcinoma. Normally, one strand of the miRNA is found much more abundantly expressed than the other strand. The abundant strands are referred to as abundant mature miRNAs or guide strand miRNAs. These mature miRNAs are highly conserved across vertebrates because they are important in regulating mRNA expression and function, and are believed to be the biologically active strands. On the other hand, the less abundant strands are less conserved with greater divergence observed across species. These less conserved strands also display greater divergence amongst members of the same family. It is believed that these less abundant strands are degraded by Ago2 becoming biologically inactive, and thus they are referred to as miRNA star (miRNA*) strands or passenger strands. The abundance of these star strands is dependent on the levels of degradation. Due to the divergence of these star strands, they are not reported as functional miRNAs. Nevertheless, further analysis found that there are some miRNA precursors that can produce two kinds of abundant mature miRNAs. Some star strands have been reported to play a regulatory role in mRNA expression. In this study, we report that the miR-17-5p and miR-17-3p were not only both abundantly expressed, but also acted in coordination to mediate the functions of miR-17. The combination of the miR-17 transgenic mouse model and the tissue culture systems in our study helped us investigate the different targets of miR-17-5p and miR-17-3p. Although functioning in different signal pathways, the three targets of miR-17 coordinately mediate the same function of this miRNA. This adds a new layer of understanding to the mechanism by which miRNA functions. In an accompanying paper, we report that one miRNA (miR-24) can target two molecules (PTPN9 and PTPRF), which coordinate the activation of EGFR and contribute to cancer metastasis (see Du et al., 2013 in this issue of *Journal of Cell Science*).

Materials and Methods

Construct generation

MicroRNA constructs that express miR-17 were designed by our lab and synthesized by Top Gene Technologies (Montreal, Canada). A cDNA sequence containing two human pre-miR-17 units was inserted into a mammalian expression vector pEGFP-N1 in the restriction enzyme sites *Bgl*II and *Hin*dIII. This plasmid was expected to simultaneously express miR-17 and GFP, producing both mature miR-17-5p and miR-17-3p. The control plasmid was the same except that the pre-miR-17 sequence was replaced with a non-related sequence (5′-atacagtactgtgataactgaagtttttggaaaagctttagttattaa-3′), serving as a mock control.

A luciferase reporter vector (pMir-Report; Ambion) was used to generate the luciferase constructs. A fragment of the 3′-untranslated region (3′-UTR) of mouse vimentin was cloned by RT-PCR using two primers, musVIM-R173p-SacI and musVIM-R173p-MluI. A fragment of the 3′-UTR of mouse PTEN was cloned by using musPten3084-R17-SacI and musPten3084-R17-MluI. Thirdly, a fragment of the 3′-UTR of mouse GalNT7 was cloned by using musGalNT7-R17*-SacI and musGalNT7-R17*-MluI. The PCR products were then digested with *Sac*I and *Mlu*I and the fragments were inserted into a *Sac*I- and *Mlu*I-opened pMir-Report Luciferase vector to obtain the luciferase constructs, Luc-Vim, Luc-PTEN and Luc-GalNT7, respectively. To serve as a negative control, a non-related sequence was amplified from the coding sequence of the chicken versican G3 domain using two primers, chver10051SpeI and chver10350SacI. We do not expect any endogenous miRNA to bind to this fragment as it is in a coding region.

To study the functions of the target proteins in miR17-regulated cell activities, vimentin and PTEN expression plasmids were purchased from Origene. We used these plasmids to generate retrovirus expression constructs. The GalNT7 cDNA containing the coding sequence was from ATCC. The PCR products of vimentin and PTEN were digested with *Bam*HI and *Sal*I while the PCR product of GalNT7 was digested with *Bcl*I and *Sal*I. The digested vimentin and PTEN fragments were then inserted into a *Bam*HI- and *Sal*I-opened pBABE vector while the digested GalNT7 fragment was inserted into the *Sal*I- and *Bam*HI-opened vector.

Cell proliferation and survival assays

HepG2 cells (obtained from ATCC) stably transfected with miR-17 or GFP were seeded onto 12-well tissue culture plates in Dulbecco's modified Eagle's medium (DMEM) containing 5% fetal bovine serum (FBS) and maintained at 37℃ for 2, 5 and 7 days. The culture medium was removed and the cells were washed with PBS. The cells were harvested and cell numbers were determined with a Coulter counter. For survival assay, the cells were seeded on 35-mm culture dishes in serum-free DMEM, and incubated for different time periods. To modulate protein expression, a number of siRNAs, miRNA inhibitors and miRNA mimics were purchased from GenePharma (Shanghai, China).

Colony formation in soft agarose gel

One thousand cells were mixed in 0.3% low-melting agarose (Seaplaque, FMC) in DMEM supplemented with 10% FBS and plated on 0.66% agarose-coated six-well tissue culture plates, which prevented attachment of cells to the plates. The culture medium was replaced with 0.5 ml DMEM containing 10% FBS twice a week. Four weeks after cell inoculation, colonies were examined and photographed under a light microscope.

Tumorigenicity assays in nude mice

Five-week-old CD1 strain nude mice were injected with the miR-17- or vector-transfected HepG2 cells at a cell number of 5×10^6 cells/100 µl PBS per mouse. The assay was performed as described previously (LaPierre et al., 2007; Wu et al., 2004). Immunohistochemistry was performed on 5 µm paraffin sections mounted on charged slides. The sections were stained with Hematoxylin and Eosin (H&E), and immunostained with CD34 to detect blood vessels. Sections were also immunostained for expression of miR-17 targets including vimentin, PTEN and GalNT7. As well, sections were subjected to immunohistochemistry analysis for expression of markers of hepatocellular carcinoma including AFP, Ki67, CD34, p53 and glypican-3.

Cell migration assay

Cells in DMED containing 5% FBS were seeded at 70% confluence onto tissue culture plates and incubated at 37℃ for 24 hours. The confluent monolayer was subjected to migration assay as described previously (Rutnam and Yang, 2012b).

Capillary formation assay

Vector- or miR17-transfected YPEN cells were grown to ~80% confluent and then harvested from the plates by 0.05% trypsin with 0.53 mM EDTA. The cells were recovered by centrifugation, washed three times with IMDM, suspended in this medium at a density of 4×10^4 cells/ml, and inoculated to matrix gel-coated eight-chamber culture slides. The culture slides were pre-coated with 1% sterile agarose, and then coated with 100 µl Matrigel on top of the agarose gel. They were then air dried at 37℃ for 10 minutes before being used for cell inoculation.

Immunohistochemistry

Organs were freshly fixed in 10% neutral buffered formalin overnight, immersed in 70% ethanol, embedded in paraffin, and sectioned by a microtome (Leica RM2255). Sections (4 µm thickness) were deparaffinized in two changes of xylene for 5 minutes each and rehydrated by placing the slides three times in 100% ethanol, 3 minutes each time. Endogenous peroxidase activity was blocked by incubating the sections in 3% H_2O_2 solution in methanol at 4℃ for 20 minutes. The sections were rinsed in TBS twice, 5 minutes each time. Antigen retrieval to unmask antigenic epitope was performed by heating the sections in sodium citrate buffer (pH 6.0) in a microwave pressure cooker for 4 minutes. Non-specific reactions with cellular proteins were blocked with 10% normal goat serum at room temperature for 30 minutes. The slides were then incubated in a humidified chamber at 4℃ overnight with primary antibody solution (primary antibody in TBS containing 10% normal goat serum and 1% BSA), washed three times in TBS, 5 minutes each time. They were then incubated with secondary antibody solution at 37℃ for 45 minutes and with ABC (Vector labs) in the same conditions, and stained with DAB according to manufacturer's protocols. The slides were subsequently countered stained with Mayer's Hematoxylin followed by slide mounting.

Western blot analysis

Protein lysates containing vimentin, PTEN, and GalNT7 were subjected to SDS-PAGE-western blot assays using the method described previously (Cao et al., 2000).

Luciferase assay

U343 cells were cultured on 24-well tissue plates in DMEM containing 10% FBS. The cultures were maintained at 37℃ and co-transfected with the luciferase reporter constructs and miRNAs mimics using Lipofectamine 2000. The cells were then collected and lysed with luciferase-specific lysis buffer from a Luciferase Assay Kit (Promega, Nepean, ON, Canada). Mixtures of cell lysates were centrifuged at 5000 rpm for 5 minutes. The supernatant were transferred into 96-well plates for luciferase activity measurement. In order to measure luciferase activity, the luciferase assay reagent was added to each well and luciferase activities were detected by using a luminescence counter (Parkard, Perkin Elmer, Woodbridge, ON, Canada). Acting as the internal control of β-gal activities, 90 µl of assay reagent (4 mg/ml ortho-nitrophenyl-β-galactoside, 0.5 M $MgSO_4$, β-mercaptomethanol and 0.4 M sodium phosphate buffer) was added to each well. The plates were then incubated at 37℃ for 1 hour. The absorbance at 410 nm was measured by using a microplate reader (Bio-Tek Instruments Inc., Winooski, VT, USA).

Real-time PCR

For mature miRNA analysis, total RNA was extracted with the mirVana miRNA Isolation Kit (Ambion) according to the manufacturer's instructions. The total RNA was extracted from $\sim1\times10^6$ cells or ~0.05 ***g*** tissues, and was followed by performing cDNA synthesis using 1 µg RNA. Successive PCR was performed by QuantiMir-RT Kit using 1 µl cDNA as a template (Qiagen, miScript Reverse Transcription Kit, cat no. 218060; miScript Primer Assay, cat no. 218411; miScriptSYBR GreenPCR Kit, cat no. 218073). The primers specific for mature miR-17-5p and miR-17-3p were purchased from Qiagen. The primers used as real-time PCR controls were human-U6RNAf and Human-U6RNAr. The primers EGFP981F and EGFP-CApaI were used to detect GFP expression. Primers used as controls were Hu-Gapdh421F and Hu-Gapdh720R (for human cell lines). For the vimentin, PTEN and GalNT7 mRNA levels, total RNA was extracted by using the RNeasy mini kit (Qiagen). After determining RNA concentrations, 1 µg of total RNA was used in the SuperScript II reverse transcription reaction by using random primers and by following the company's instruction (Invitrogen). The sense and antisense primers used in PCR amplification of the three target genes and GAPDH are listed in supplementary material Table S2. PCR was carried out at 94℃ followed by 25 cycles at 94℃, 58℃ and 72℃. The reaction was terminated with a product extension step at 72℃ for 10 minutes. Ten microliter aliquots of PCR products were loaded with loading buffer and separated on 1.5% agarose gel for DNA analysis.

Statistical analysis

The results (mean values ± s.e.m.) of all the experiments were subjected to statistical analysis by Student's *t*-test. The level of significance was set at $P<0.05$ and $P<0.01$.

Acknowledgements

The authors thank G. Knowles, J. Sun, Y. Amemiya, W. Yang, H. Cadieux-Pitre, S. Gatchell, and S. P. Yee for technical assistance and J. Yang for editing the manuscript.

Author contributions

S.W.S. performed all western blot analyses, most of the cell biology experiments and luciferase assays, was involved in tumor formation assays, organized all tissue samples, and was involved in data analysis and paper writing. L.F. was involved in animal dissecting analysis, directed pathological analysis and in some immunostaining. T.S. performed most of the immunohistochemistry analysis. Z.D. performed real-time PCR analyses, colony formation assays, and was involved in tumor formation assay and genotyping. Z.J.R. helped with flourescent and immunostaining, for sample collection and paper writing. X.Y. performed some immunostaining. W.W.D. was involved in genotyping. W.Y.L. helped with sample collection. J.W.X. was involved in work using transgenic mice. B.B.Y. designed and supervised the project, analyzed the results and wrote the paper.

Funding

This work was supported by the Canadian Institutes of Health Research [grant numbers MOP-102635 and MOP-111171 to B.B.Y.] and a Career Investigator Award from the Heart and Stroke Foundation of Ontario [grant number CI 5958 to B.B.Y.].

Supplementary material available online at
http://jcs.biologists.org/lookup/suppl/doi:10.1242/jcs.122895/-/DC1

References

Altuvia, Y., Landgraf, P., Lithwick, G., Elefant, N., Pfeffer, S., Aravin, A., Brownstein, M. J., Tuschl, T. and Margalit, H. (2005). Clustering and conservation patterns of human microRNAs. *Nucleic Acids Res.* **33**, 2697-2706.

Bonauer, A. and Dimmeler, S. (2009). The microRNA-17-92 cluster: still a miRacle? *Cell Cycle* **8**, 3866-3873.

Cao, L., Yao, Y., Lee, V., Kiani, C., Spaner, D., Lin, Z., Zhang, Y., Adams, M. E. and Yang, B. B. (2000). Epidermal growth factor induces cell cycle arrest and apoptosis of squamous carcinoma cells through reduction of cell adhesion. *J. Cell. Biochem.* **77**, 569-583.

Connolly, E., Melegari, M., Landgraf, P., Tchaikovskaya, T., Tennant, B. C., Slagle, B. L., Rogler, L. E., Zavolan, M., Tuschl, T. and Rogler, C. E. (2008). Elevated expression of the miR-17-92 polycistron and miR-21 in hepadnavirus-associated hepatocellular carcinoma contributes to the malignant phenotype. *Am. J. Pathol.* **173**, 856-864.

Dang, C. V. (2009). MYC, microRNAs and glutamine addiction in cancers. *Cell Cycle* **8**, 3243-3245.

Deng, M., Tang, H., Zhou, Y., Zhou, M., Xiong, W., Zheng, Y., Ye, Q., Zeng, X., Liao, Q., Guo, X. et al. (2011). miR-216b suppresses tumor growth and invasion by targeting KRAS in nasopharyngeal carcinoma. *J. Cell Sci.* **124**, 2997-3005.

Denli, A. M., Tops, B. B., Plasterk, R. H., Ketting, R. F. and Hannon, G. J. (2004). Processing of primary microRNAs by the Microprocessor complex. *Nature* **432**, 231-235.

Du, W. W., Fang, L., Li, M., Yang, X., Liang, Y., Peng, C., Qian, W., O'Malley, Y. Q., Askeland, R. W., Sugg, S. et al. (2013). MicroRNA miR-24 enhances tumor invasion and metastasis by targeting PTPN9 and PTPRF to promote EGF signaling. *J. Cell Sci.* **126**, 1440-1453.

Fang, L., Deng, Z., Shatseva, T., Yang, J., Peng, C., Du, W. W., Yee, A. J., Ang, L. C., He, C., Shan, S. W. et al. (2011). MicroRNA miR-93 promotes tumor growth and angiogenesis by targeting integrin-β8. *Oncogene* **30**, 806-821.

Fang, L., Du, W. W., Yang, W., Rutnam, Z. J., Peng, C., Li, H., O'Malley, Y. Q., Askeland, R. W., Sugg, S., Liu, M. et al. (2012). MiR-93 enhances angiogenesis and metastasis by targeting LATS2. *Cell Cycle* **11**, 4352-4365.

Gaziel-Sovran, A., Segura, M. F., Di Micco, R., Collins, M. K., Hanniford, D., Vega-Saenz de Miera, E., Rakus, J. F., Dankert, J. F., Shang, S., Kerbel, R. S. et al. (2011). miR-30b/30d regulation of GalNAc transferases enhances invasion and immunosuppression during metastasis. *Cancer Cell* **20**, 104-118.

Geary, R. S., Wancewicz, E., Matson, J., Pearce, M., Siwkowski, A., Swayze, E. and Bennett, F. (2009). Effect of dose and plasma concentration on liver uptake and pharmacologic activity of a 2′-methoxyethyl modified chimeric antisense oligonucleotide targeting PTEN. *Biochem. Pharmacol.* **78**, 284-291.

Goljanek-Whysall, K., Pais, H., Rathjen, T., Sweetman, D., Dalmay, T. and Münsterberg, A. (2012). Regulation of multiple target genes by miR-1 and miR-206 is pivotal for C2C12 myoblast differentiation. *J. Cell Sci.* **125**, 3590-3600.

Guo, L. and Lu, Z. (2010). The fate of miRNA* strand through evolutionary analysis: implication for degradation as merely carrier strand or potential regulatory molecule? *PLoS ONE* **5**, e11387.

Guo, L., Li, H., Liang, T., Lu, J., Yang, Q., Ge, Q. and Lu, Z. (2012). Consistent isomiR expression patterns and 3′ addition events in miRNA gene clusters and families implicate functional and evolutionary relationships. *Mol. Biol. Rep.* **39**, 6699-6706.

Hayashita, Y., Osada, H., Tatematsu, Y., Yamada, H., Yanagisawa, K., Tomida, S., Yatabe, Y., Kawahara, K., Sekido, Y. and Takahashi, T. (2005). A polycistronic microRNA cluster, miR-17-92, is overexpressed in human lung cancers and enhances cell proliferation. *Cancer Res.* **65**, 9628-9632.

Horie, Y., Suzuki, A., Kataoka, E., Sasaki, T., Hamada, K., Sasaki, J., Mizuno, K., Hasegawa, G., Kishimoto, H., Iizuka, M. et al. (2004). Hepatocyte-specific Pten deficiency results in steatohepatitis and hepatocellular carcinomas. *J. Clin. Invest.* **113**, 1774-1783.

Huang, Q., Gumireddy, K., Schrier, M., le Sage, C., Nagel, R., Nair, S., Egan, D. A., Li, A., Huang, G., Klein-Szanto, A. J. et al. (2008). The microRNAs miR-373 and miR-520c promote tumour invasion and metastasis. *Nat. Cell Biol.* **10**, 202-210.

Jeyapalan, Z., Deng, Z., Shatseva, T., Fang, L., He, C. and Yang, B. B. (2011). Expression of CD44 3′-untranslated region regulates endogenous microRNA functions in tumorigenesis and angiogenesis. *Nucleic Acids Res.* **39**, 3026-3041.

Kahai, S., Lee, S. C., Lee, D. Y., Yang, J., Li, M., Wang, C. H., Jiang, Z., Zhang, Y., Peng, C. and Yang, B. B. (2009). MicroRNA miR-378 regulates nephronectin expression modulating osteoblast differentiation by targeting GalNT-7. *PLoS ONE* **4**, e7535.

Kiriakidou, M., Tan, G. S., Lamprinaki, S., De Planell-Saguer, M., Nelson, P. T. and Mourelatos, Z. (2007). An mRNA m7G cap binding-like motif within human Ago2 represses translation. *Cell* **129**, 1141-1151.

Klymkowsky, M. W., Bachant, J. B. and Domingo, A. (1989). Functions of intermediate filaments. *Cell Motil. Cytoskeleton* **14**, 309-331.

Kutay, H., Bai, S., Datta, J., Motiwala, T., Pogribny, I., Frankel, W., Jacob, S. T. and Ghoshal, K. (2006). Downregulation of miR-122 in the rodent and human hepatocellular carcinomas. *J. Cell. Biochem.* **99**, 671-678.

Landais, S., Landry, S., Legault, P. and Rassart, E. (2007). Oncogenic potential of the miR-106-363 cluster and its implication in human T-cell leukemia. *Cancer Res.* **67**, 5699-5707.

LaPierre, D. P., Lee, D. Y., Li, S. Z., Xie, Y. Z., Zhong, L., Sheng, W., Deng, Z. and Yang, B. B. (2007). The ability of versican to simultaneously cause apoptotic resistance and sensitivity. *Cancer Res.* **67**, 4742-4750.

Lee, Y., Ahn, C., Han, J., Choi, H., Kim, J., Yim, J., Lee, J., Provost, P., Rådmark, O., Kim, S. et al. (2003). The nuclear RNase III Drosha initiates microRNA processing. *Nature* **425**, 415-419.

Lee, D. Y., Deng, Z., Wang, C. H. and Yang, B. B. (2007). MicroRNA-378 promotes cell survival, tumor growth, and angiogenesis by targeting SuFu and Fus-1 expression. *Proc. Natl. Acad. Sci. USA* **104**, 20350-20355.

Lee, D. Y., Shatseva, T., Jeyapalan, Z., Du, W. W., Deng, Z. and Yang, B. B. (2009). A 3′-untranslated region (3'UTR) induces organ adhesion by regulating miR-199a* functions. *PLoS ONE* **4**, e4527.

Lee, S. C., Fang, L., Wang, C. H., Kahai, S., Deng, Z. and Yang, B. B. (2011). A non-coding transcript of nephronectin promotes osteoblast differentiation by modulating microRNA functions. *FEBS Lett.* **585**, 2610-2616.

Li, Y., Tan, W., Neo, T. W., Aung, M. O., Wasser, S., Lim, S. G. and Tan, T. M. (2009). Role of the miR-106b-25 microRNA cluster in hepatocellular carcinoma. *Cancer Sci.* **100**, 1234-1242.

Luo, L., Ye, G., Nadeem, L., Fu, G., Yang, B. B., Honarparvar, E., Dunk, C., Lye, S. and Peng, C. (2012). MicroRNA-378a-5p promotes trophoblast cell survival, migration and invasion by targeting Nodal. *J. Cell Sci.* **125**, 3124-3132.

Ma, L., Teruya-Feldstein, J. and Weinberg, R. A. (2007). Tumour invasion and metastasis initiated by microRNA-10b in breast cancer. *Nature* **449**, 682-688.

Matranga, C., Tomari, Y., Shin, C., Bartel, D. P. and Zamore, P. D. (2005). Passenger-strand cleavage facilitates assembly of siRNA into Ago2-containing RNAi enzyme complexes. *Cell* **123**, 607-620.

Matsubara, H., Takeuchi, T., Nishikawa, E., Yanagisawa, K., Hayashita, Y., Ebi, H., Yamada, H., Suzuki, M., Nagino, M., Nimura, Y. et al. (2007). Apoptosis induction by antisense oligonucleotides against miR-17-5p and miR-20a in lung cancers overexpressing miR-17-92. *Oncogene* **26**, 6099-6105.

Mendell, J. T. (2005). MicroRNAs: critical regulators of development, cellular physiology and malignancy. *Cell Cycle* **4**, 1179-1184.

Nohata, N., Hanazawa, T., Enokida, H. and Seki, N. (2012). microRNA-1/133a and microRNA-206/133b clusters: dysregulation and functional roles in human cancers. *Oncotarget* **3**, 9-21.

O'Donnell, K. A., Wentzel, E. A., Zeller, K. I., Dang, C. V. and Mendell, J. T. (2005). c-Myc-regulated microRNAs modulate E2F1 expression. *Nature* **435**, 839-843.

Rutnam, Z. J. and Yang, B. B. (2012a). The involvement of microRNAs in malignant transformation. *Histol. Histopathol.* **27**, 1263-1270.

Rutnam, Z. J. and Yang, B. B. (2012b). The non-coding 3′ UTR of CD44 induces metastasis by regulating extracellular matrix functions. *J. Cell Sci.* **125**, 2075-2085.

Sarria, A. J., Panini, S. R. and Evans, R. M. (1992). A functional role for vimentin intermediate filaments in the metabolism of lipoprotein-derived cholesterol in human SW-13 cells. *J. Biol. Chem.* **267**, 19455-19463.

Shan, S. W., Lee, D. Y., Deng, Z., Shatseva, T., Jeyapalan, Z., Du, W. W., Zhang, Y., Xuan, J. W., Yee, S. P., Siragam, V. et al. (2009). MicroRNA MiR-17 retards tissue growth and represses fibronectin expression. *Nat. Cell Biol.* **11**, 1031-1038.

Shatseva, T., Lee, D. Y., Deng, Z. and Yang, B. B. (2011). MicroRNA miR-199a-3p regulates cell proliferation and survival by targeting caveolin-2. *J. Cell Sci.* **124**, 2826-2836.

Smits, M., Nilsson, J., Mir, S. E., van der Stoop, P. M., Hulleman, E., Niers, J. M., de Witt Hamer, P. C., Marquez, V. E., Cloos, J., Krichevsky, A. M. et al. (2010). miR-101 is down-regulated in glioblastoma resulting in EZH2-induced proliferation, migration, and angiogenesis. *Oncotarget* **1**, 710-720.

Sylvestre, Y., De Guire, V., Querido, E., Mukhopadhyay, U. K., Bourdeau, V., Major, F., Ferbeyre, G. and Chartrand, P. (2007). An E2F/miR-20a autoregulatory feedback loop. *J. Biol. Chem.* **282**, 2135-2143.

Viticchiè, G., Lena, A. M., Latina, A., Formosa, A., Gregersen, L. H., Lund, A. H., Bernardini, S., Mauriello, A., Miano, R., Spagnoli, L. G. et al. (2011). MiR-203 controls proliferation, migration and invasive potential of prostate cancer cell lines. *Cell Cycle* **10**, 1121-1131.

Volinia, S., Calin, G. A., Liu, C. G., Ambs, S., Cimmino, A., Petrocca, F., Visone, R., Iorio, M., Roldo, C., Ferracin, M. et al. (2006). A microRNA expression signature of human solid tumors defines cancer gene targets. *Proc. Natl. Acad. Sci. USA* **103**, 2257-2261.

Wang, C. H., Lee, D. Y., Deng, Z., Jeyapalan, Z., Lee, S. C., Kahai, S., Lu, W. Y., Zhang, Y. and Yang, B. B. (2008a). MicroRNA miR-328 regulates zonation morphogenesis by targeting CD44 expression. *PLoS ONE* **3**, e2420.

Wang, Q., Li, Y. C., Wang, J., Kong, J., Qi, Y., Quigg, R. J. and Li, X. (2008b). miR-17-92 cluster accelerates adipocyte differentiation by negatively regulating tumor-suppressor Rb2/p130. *Proc. Natl. Acad. Sci. USA* **105**, 2889-2894.

Wu, Y., Chen, L., Cao, L., Sheng, W. and Yang, B. B. (2004). Overexpression of the C-terminal PG-M/versican domain impairs growth of tumor cells by intervening in the interaction between epidermal growth factor receptor and beta1-integrin. *J. Cell Sci.* **117**, 2227-2237.

Xiao, C., Srinivasan, L., Calado, D. P., Patterson, H. C., Zhang, B., Wang, J., Henderson, J. M., Kutok, J. L. and Rajewsky, K. (2008). Lymphoproliferative disease and autoimmunity in mice with increased miR-17-92 expression in lymphocytes. *Nat. Immunol.* **9**, 405-414.

Yang, F., Yin, Y., Wang, F., Wang, Y., Zhang, L., Tang, Y. and Sun, S. (2010). miR-17-5p Promotes migration of human hepatocellular carcinoma cells through the p38 mitogen-activated protein kinase-heat shock protein 27 pathway. *Hepatology* **51**, 1614-1623.

Ye, G., Fu, G., Cui, S., Zhao, S., Bernaudo, S., Bai, Y., Ding, Y., Zhang, Y., Yang, B. B. and Peng, C. (2011). MicroRNA 376c enhances ovarian cancer cell survival by targeting activin receptor-like kinase 7: implications for chemoresistance. *J. Cell Sci.* **124**, 359-368.

Yu, B., Zhou, S., Wang, Y., Qian, T., Ding, G., Ding, F. and Gu, X. (2012). miR-221 and miR-222 promote Schwann cell proliferation and migration by targeting LASS2 after sciatic nerve injury. *J. Cell Sci.* **125**, 2675-2683.

Zou, C., Xu, Q., Mao, F., Li, D., Bian, C., Liu, L. Z., Jiang, Y., Chen, X., Qi, Y., Zhang, X. et al. (2012). MiR-145 inhibits tumor angiogenesis and growth by N-RAS and VEGF. *Cell Cycle* **11**, 2137-2145.

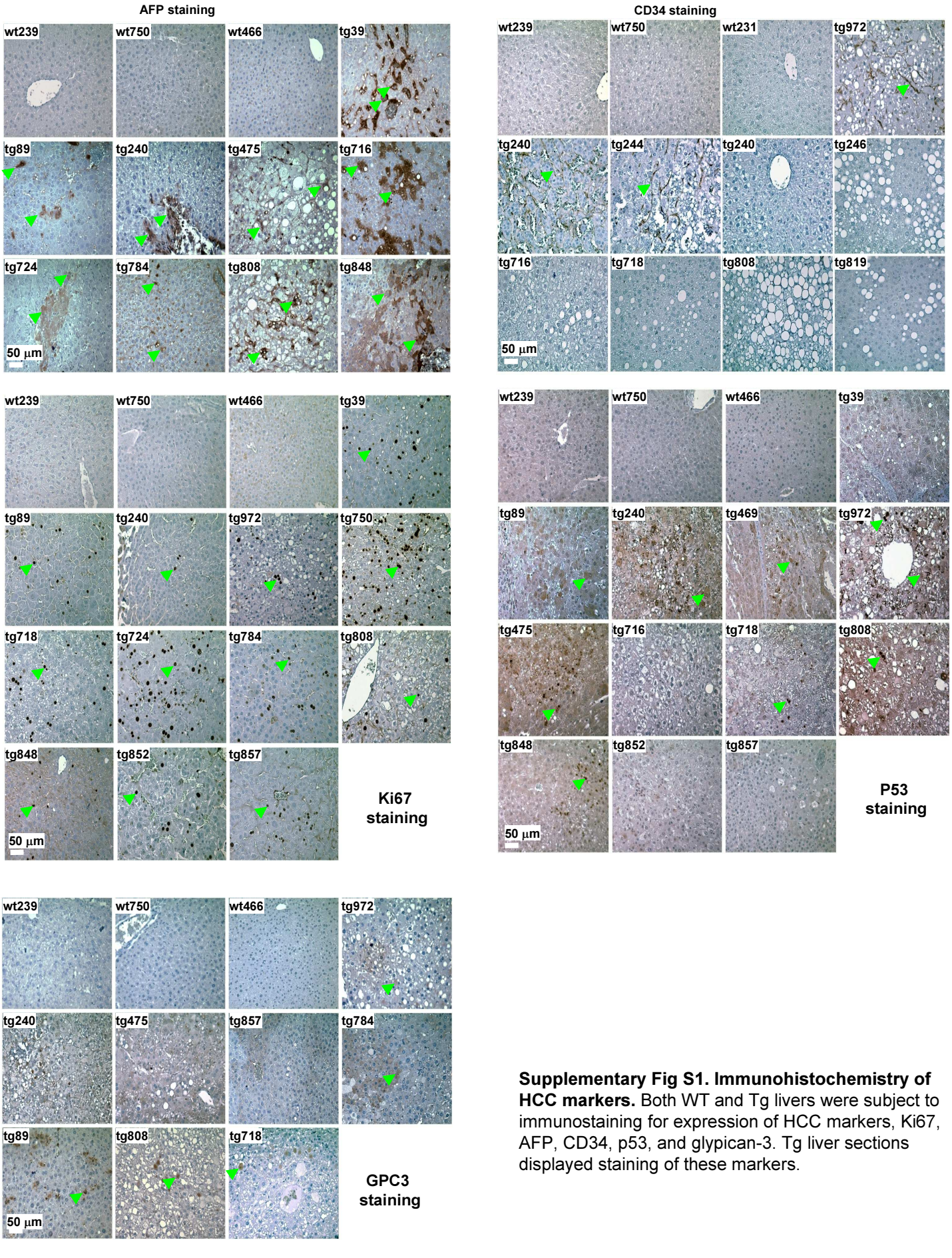

Supplementary Fig S1. Immunohistochemistry of HCC markers. Both WT and Tg livers were subject to immunostaining for expression of HCC markers, Ki67, AFP, CD34, p53, and glypican-3. Tg liver sections displayed staining of these markers.

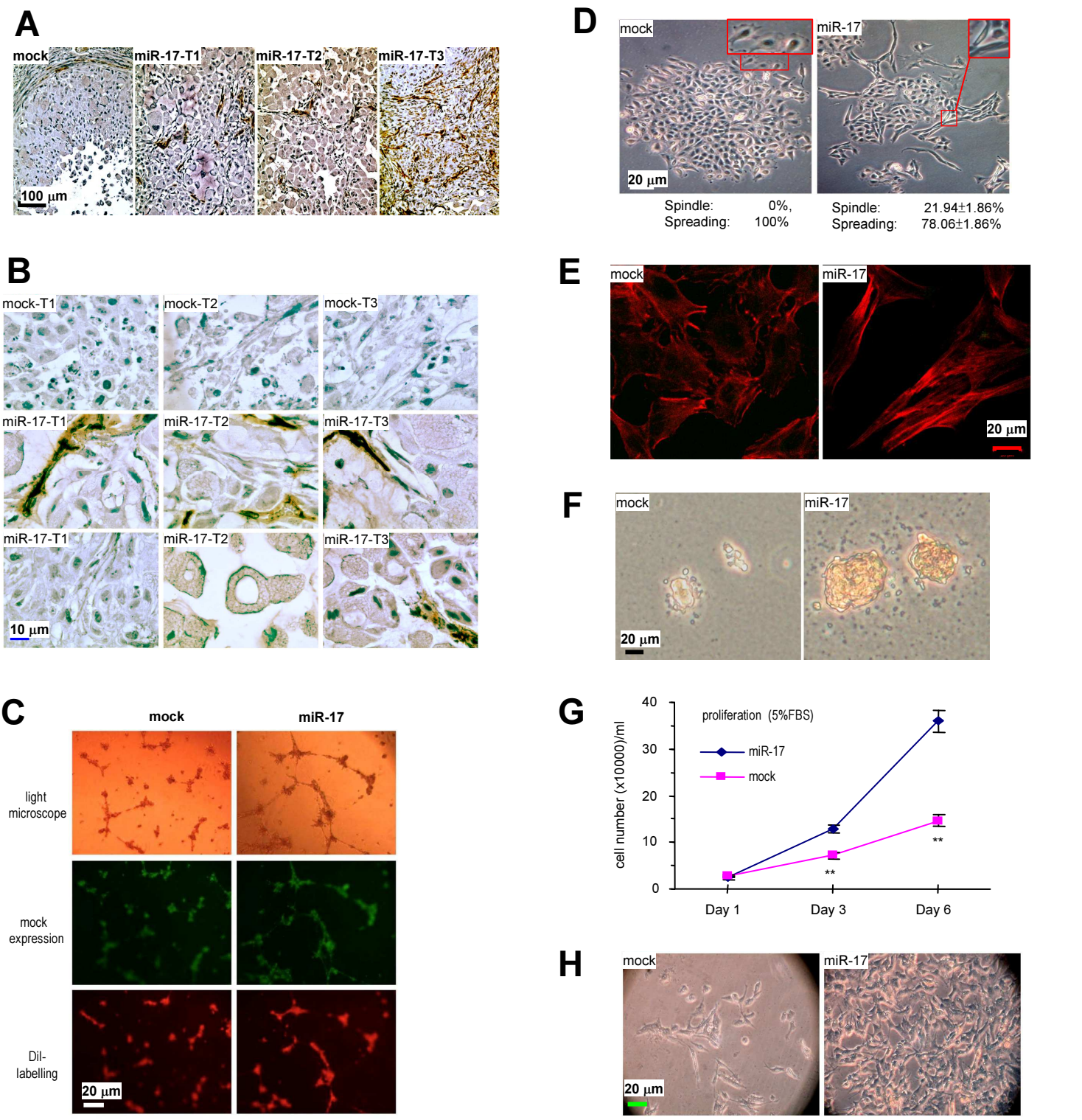

Supplementary Fig S2. Roles of miR-17 in angiogenesis and cell activities. (**A**) Tumor sections were subject to immunohistochemistry probed with anti-CD34 antibody. Expression of miR-17 construct elevated the amount of blood vessels. (**B**) Both mock- and miR-17 tumor sections were probed with anti-CD34 antibody. Blood vessels were detected in miR-17 tumors but not in mock tumors. Extensive cell death could be seen in the mock tumors but not in the miR-17 tumors. (**C**) The miR-17- and mock-transfected cells were mixed with endothelial cells YPEN, which were pre-stained with DiI dye, and inoculated in Matrigel, followed by examination of tube formation. Larger complexes and longer tubes were formed when YPEN cells were mixed with the miR-17-expressing cells compared with the mock-transfected cells. (**D**) Cell elongation was detected in the miR-17-transfected HepG2 cells as compared with mock-transfected cells. The number of spindle and spreading cells were counted and provided below the cell pictures. (**E**) The cells were also probed with anti-b-actin antibody followed by confocal microscopic examination. The miR-17-cells displayed elongated actin cytoskeleton. (**F**) Both mock- and miR-17-transfected HepG2 cells were cultured in soft agarose gel. Larger colonies were formed by miR-17-overexpressed cells. (**G**) The cells were maintained in 5% serum containing medium and the number of cells was counted on days 1, 3, and 6 to determine cell proliferation rates. MiR-17-transfected cells proliferated faster than the control cells. (**H**) Cells were maintained in serum-free conditions. Cell survival was monitored with a fluorescent microscope. Transfection with miR-17 enhanced cell survival.

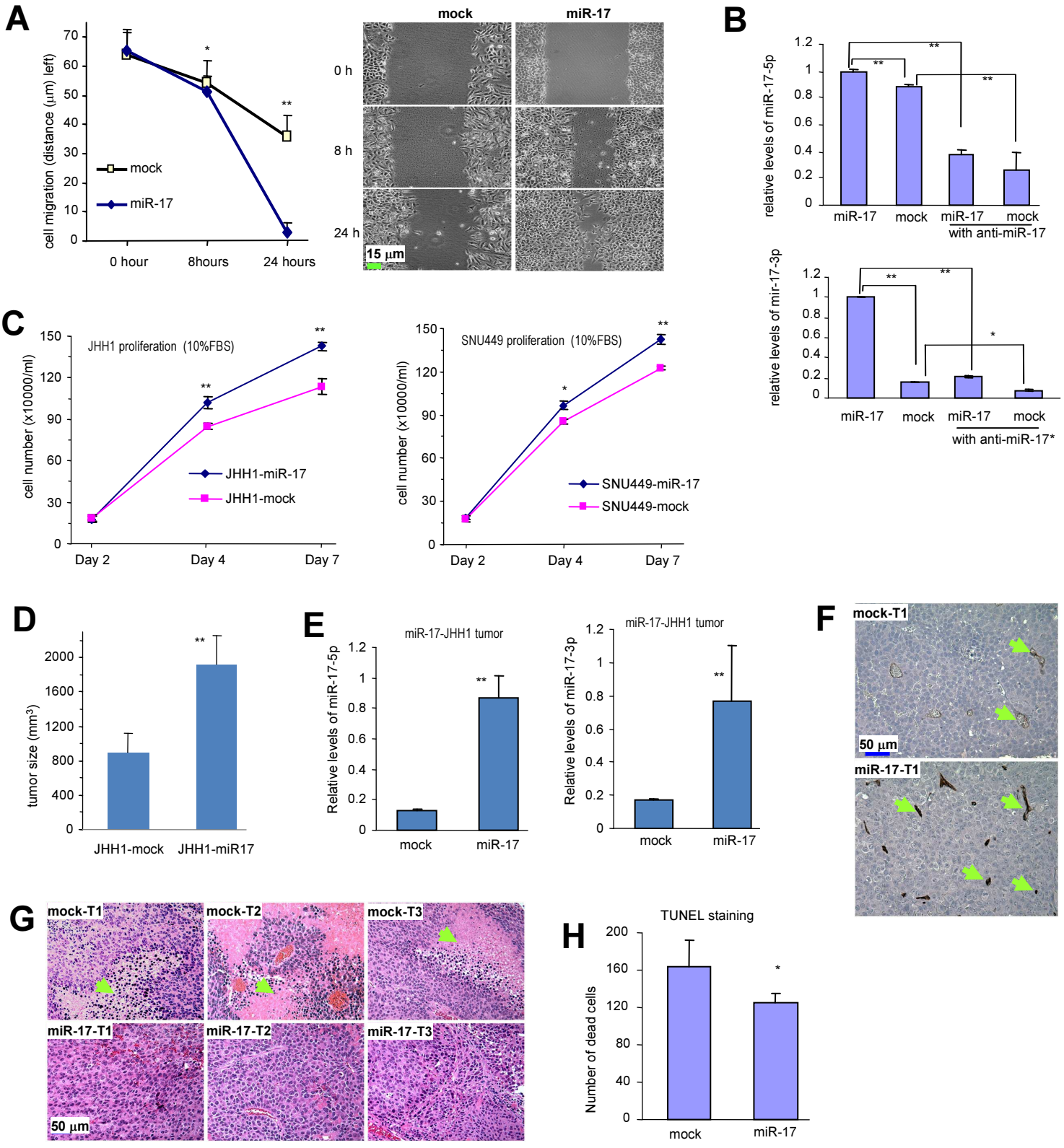

Supplementary Fig S3. Effects of miR-17 on JHH-l and SNU449 cell proliferation and tumor growth. (**A**) Left, cells were cultured for migration assay. Cells expressing miR-17 showed higher motility than the controls. Right, typical photos of cell migration are shown. (**B**) Cells were transfected with or without antisense oligos against miR-17-5p or miR-17-3p. The levels of miR-17-5p (upper) and miR-17-3p (lower) were analyzed by real-time PCR. Transfection with antisense oligos decreased miR-17-5p and miR-17-3p levels. * $p < 0.05$, ** $p < 0.01$. **(C)** JHH1 and SNU449 cells stably transfected with miR-17 or mock were subjected to proliferation assays. Expression of miR-17 promoted cell proliferation significantly more than the mock control. (**D**) The cells were injected into nude mice for tumor growth assays. Expression of miR-17 promoted tumor growth. (**E**) Expression of miR-17-5p and miR-17-3p was confirmed by real-time PCR. (**F**) Tumors sections were probed for blood vessel formation using anti-CD34 antibody. The mock-tumors showed weaker and less staining than the miR-17-tumors. (**G**) The tumor sections were also subjected to H&E staining. The tumors formed by the mock-JHHl cells displayed extensive cell death (arrows), which is less obvious in the miR-17-tumors. (**H**) Apoptotic cells in the tumor sections were analyzed by TUNEL staining. The dead cells were counted per field. Expression of miR-17 reduced tumor cell death.

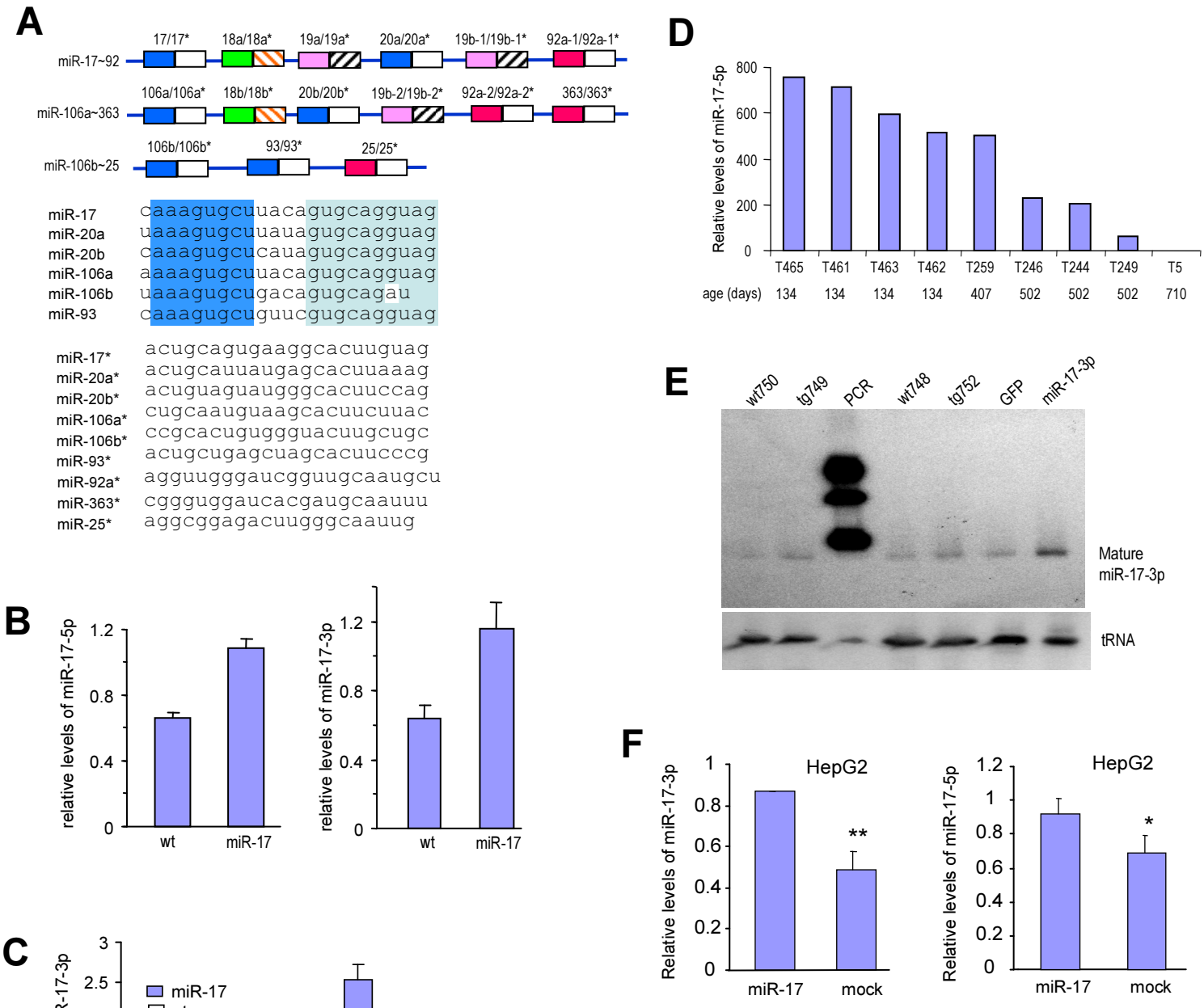

Supplementary Fig S4. Analysis of miR-17 expression in the transgenic mice. (**A**) Upper, clusters of miR-17-92, miR-106a-363 and miR-106b-25. Middle, sequence comparison of miR17 with other members harbouring the same seed sequences (highlighted). Lower, comparison of miR17-3p (miR-17*) with other miRNA* sequences in the cluster. (**B**) Expression of mature miR-17-5p and miR-17-3p were analyzed by real-time PCR using RNAs isolated from the livers of the miR-17-transgenic (Tg) and wild-type (WT) mice as indicated. Both miR-17-5p and miR-17-3p were comparably up-regulated (n = 3 PCRs. Data are mean ± s.d., * $p < 0.05$, ** $p < 0.01$.) (**C**) Expression of miR-17-5p and miR-17-3p were analyzed in miR-17 transgenic or wildtype livers, kidneys, hearts, and lungs. Both miR-17-5p and miR-17-3p were up regulated (n = 3 PCRs. Data are mean ± s.d.) (**D**) Real-time PCR analysis of miR-17-5p expression in the livers from animals of different age. (**E**) Northern blot analysis was used to detect the expression levels of miR-17-3p in HepG2 stably transfected cells, WT and Tg livers. (**F**) Expression of miR-17-5p and miR-17-3p were analyzed in HepG2 cells stably transfected with miR-17 or mock. Both miR-17-5p and miR-17-3p were up regulated (n = 3 PCRs. Data are mean ± s.d.)

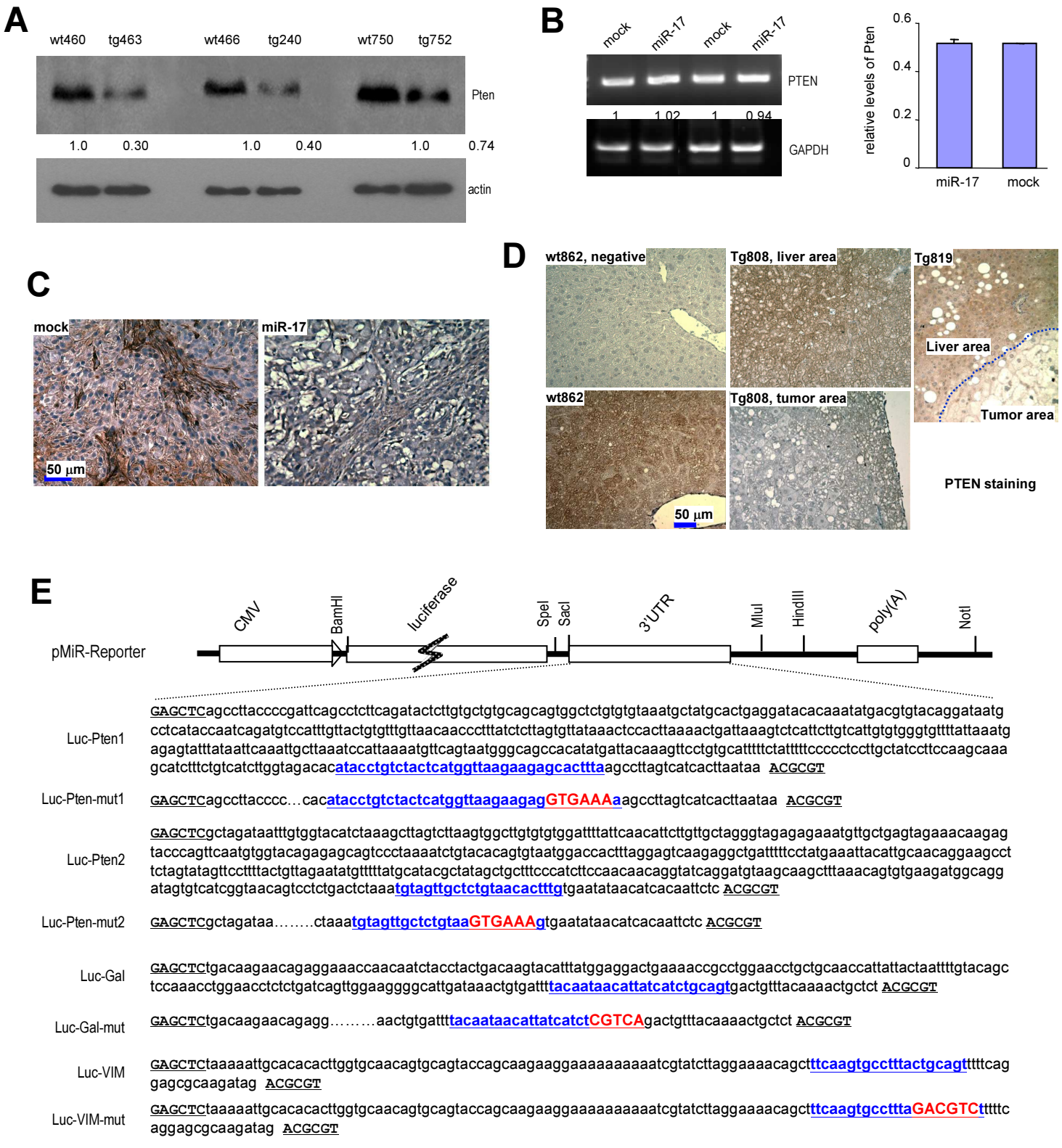

Supplementary Fig S5. MiR-17 suppressed PTEN expression. (A) PTEN protein expression was examined by western blot analysis of liver lysate from miR-17 transgenic (tg) and wild type (wt) mice and showed down-regulation of PTEN expression in the transgenic mice. (**B**) Expression of PTEN was determined with RT-PCR (left) and real-time PCR (right). No significant difference between miR-17-transfected cells and the control was detected. (**C**) The tumor sections were immunostained with anti-PTEN antibody. Tumor sections formed by the miR-17-transfected cells exhibited much lower levels of PTEN compared with the control. (**D**) Paraffin sections of miR-17 and WT livers were immunostained with an anti-PTEN antibody or the secondary antibody as a negative control. In general, PTEN staining was weaker in Tg tumors. (**E**) The 3'UTR regions of PTEN, GalNT7 and vimentin were inserted into the luciferase reporter vector pMir-Report. Mutations (red) were generated in the potential target sequence (blue).

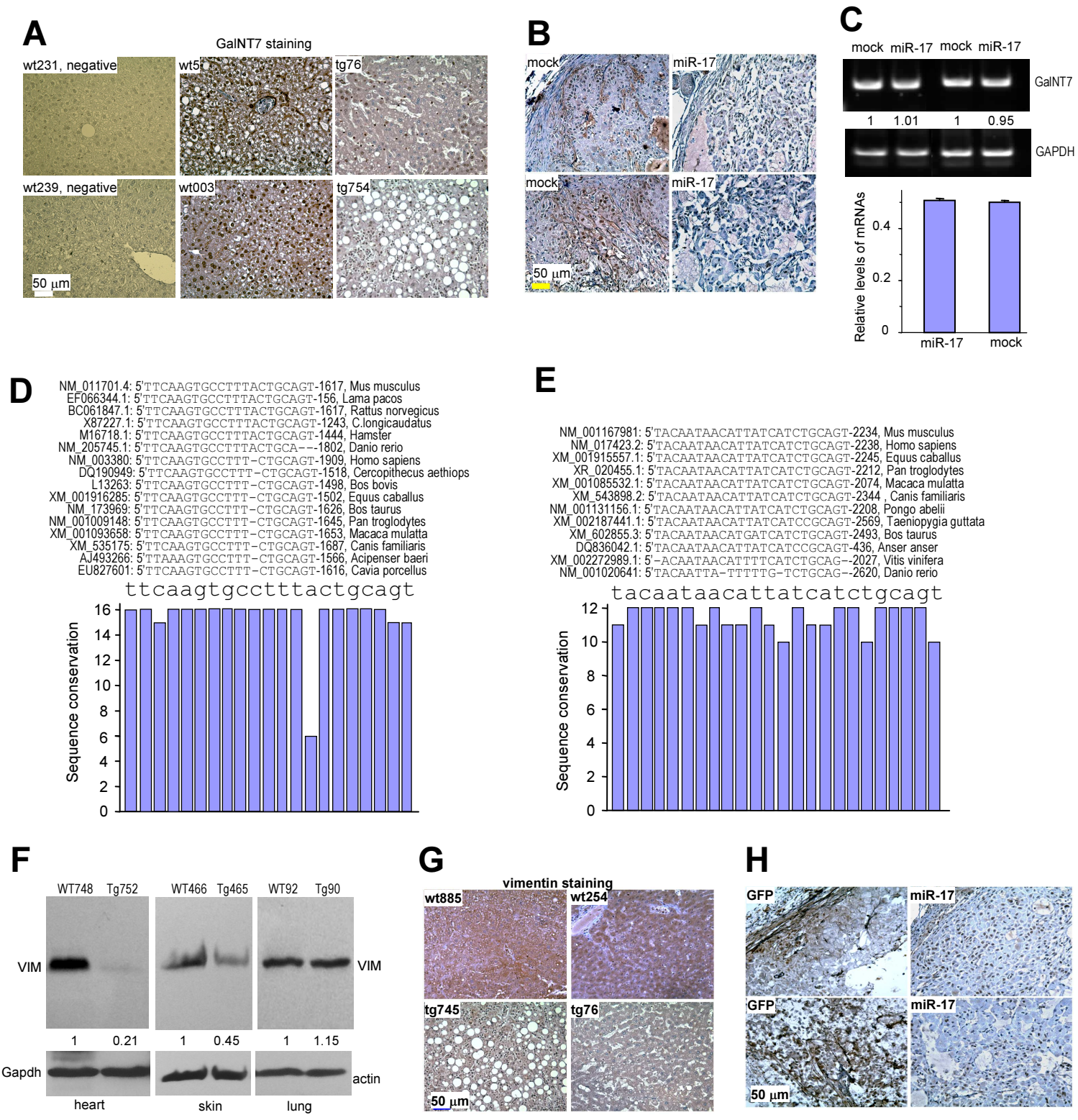

Supplementary Fig S6. MiR-17 over-expression down-regulated target levels. (**A**) Sections of Tg and WT livers were immunostained with an anti-GalNT7 antibody or with the secondary antibody as a negative control. GalNT7 staining was weaker in the Tg liver than in the WT liver. (**B**) Tumor sections were immunostained with anti-GalNT7 antibody. The miR-17 tumors exhibited lower levels of GalNT7 than mock tumors. (**C**) Expression of GalNT7 was determined with RT-PCR (upper) and real-time PCR (lower). No significant difference between miR-17-transfected cells and the control was detected. (**D**) Upper, alignment of the miR-17-3p target site in GalNT7 across different species. Lower, conservation of the sequences is shown across all species. (**E**) Top, alignment of the miR-17-3p target site in vimentin across different species. Bottom, conservation of the sequences is shown across all species. (**F**) Western blot analysis showing down-regulation of vimentin in miR-17 transgenic heart and skin. (**G**) Immunostaining for vimentin expression was performed on both Tg and WT liver sections. Tg liver exhibited lower levels of vimentin expression than the WT liver. (**H**) Tumor sections were immunostained with anti-vimentin antibody. Lower levels of vimentin were present in the miR-17 tumors than in the GFP tumors.

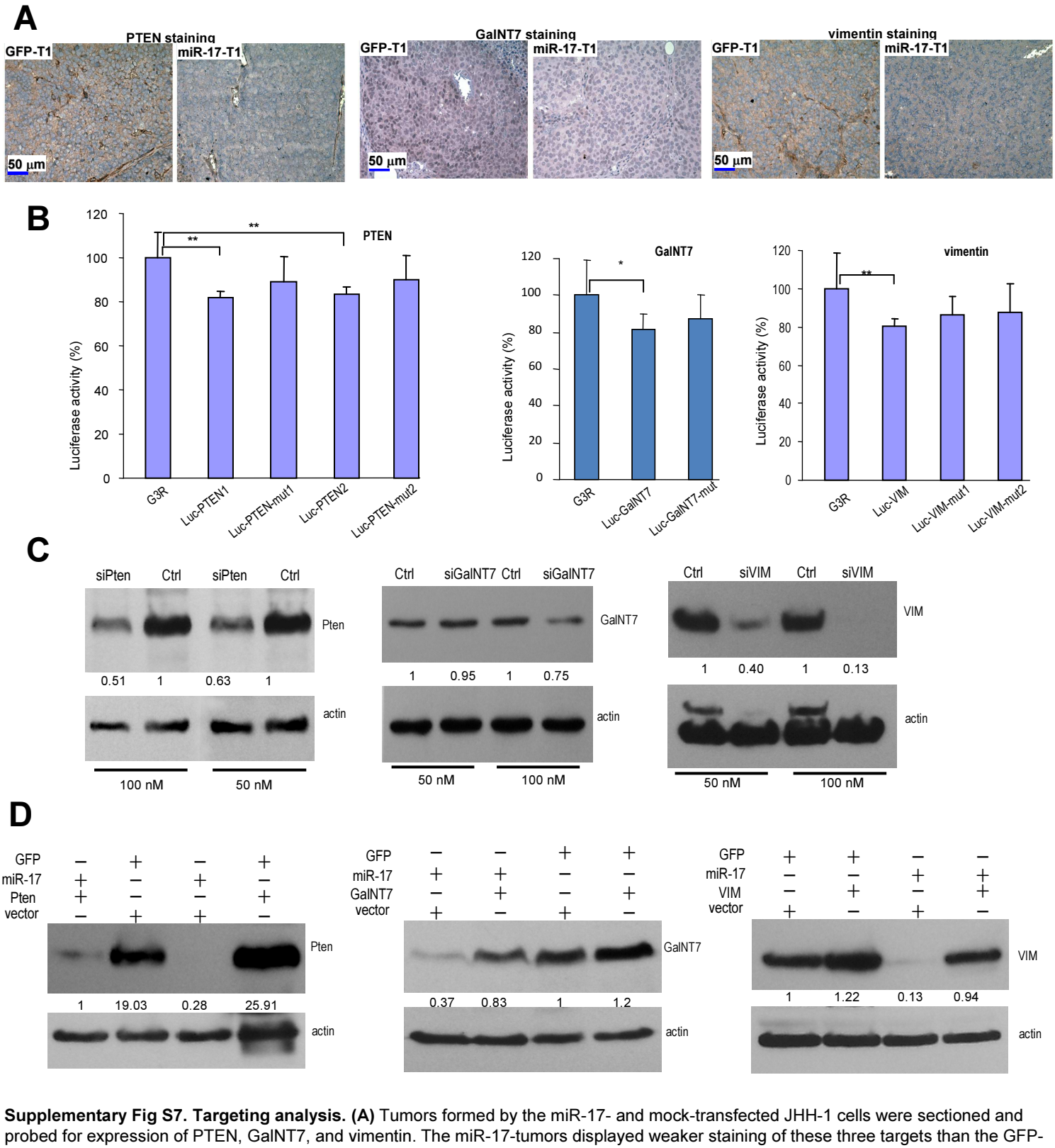

Supplementary Fig S7. Targeting analysis. (A) Tumors formed by the miR-17- and mock-transfected JHH-1 cells were sectioned and probed for expression of PTEN, GalNT7, and vimentin. The miR-17-tumors displayed weaker staining of these three targets than the GFP-tumors. **(B)** Cells were transfected with luciferase constructs harboring the 3'UTRs of PTEN, GalNT7, and vimentin to test the activities of endogenous miR-17. Controls were the constructs, which harbored the mutations of miR-17 target sites, or which contained an unrelated sequence (G3R). Luciferase activities decreased when the luciferase constructs contained the miR-17 target sites, as compared with the control constructs. **(C)** Cell lysates prepared from HepG2 cells transiently transfected with control oligos or siRNA oligos targeting PTEN, GalNT7, and vimentin were subjected to western blot analysis to confirm silencing of these proteins. Two different concentrations of oligos were used. PTEN and vimentin expressions were repressed by both concentrations of siRNA transfection (50 nM and 100 nM), while the GalNT7 was repressed when transfected with 100 nM siRNA. Staining for actin expression from the same membrane confirmed equal loading. **(D)** Both mock and miR-17-transfected HepG2 cells were transfected with (+) or without (-) control vector or expression constructs to analyze up-regulation of PTEN, GalNT7, and vimentin expression. All 3 targets were repressed when miR-17 was overexpressed in HepG2 cells. After transfecting PTEN, GalNT7 or vimentin into the cells, their respective target proteins were re-introduced in miR-17-HepG2 cells.

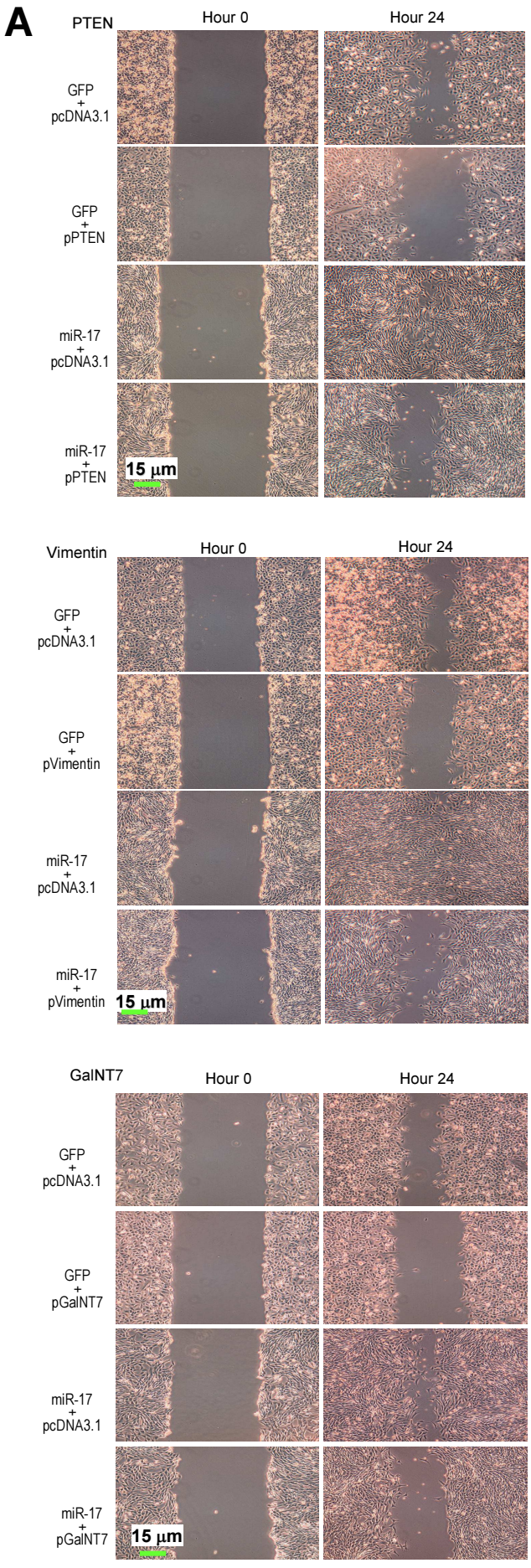

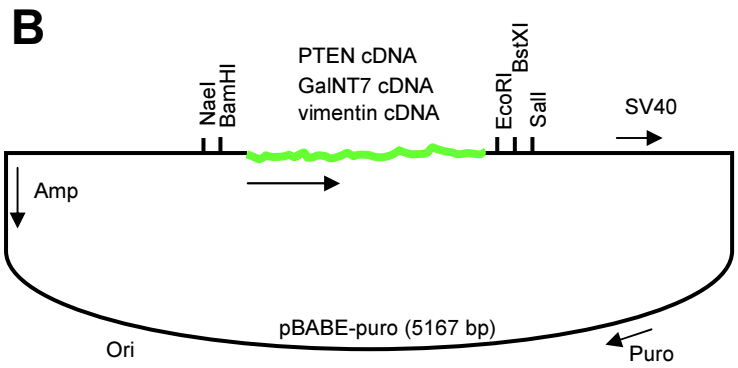

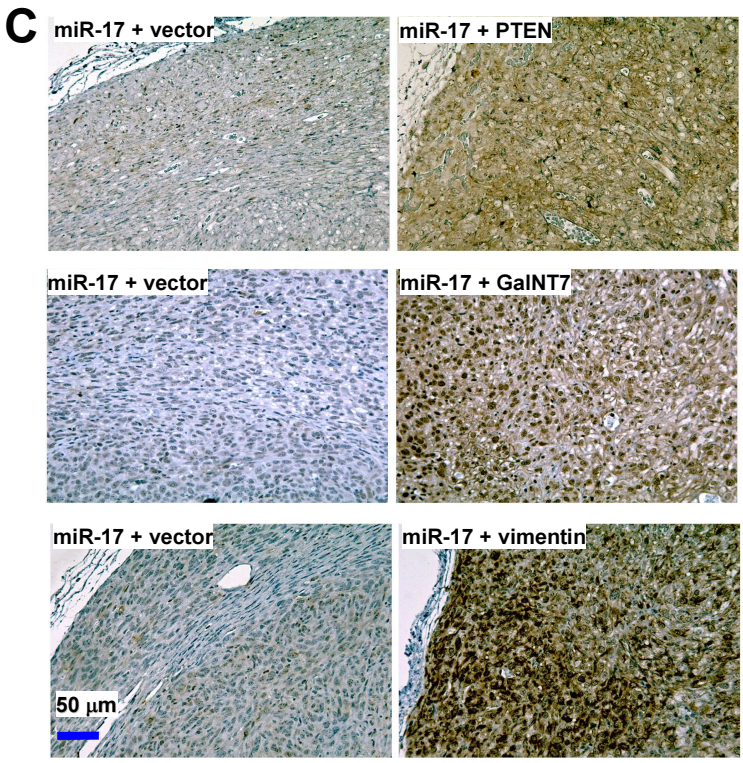

Supplementary Fig S8. Rescue experiments. (**A**) GFP- and miR-17-transfected cells were transiently transfected with expression constructs of PTEN, GalNT7, vimentin, and pcDNA3.1 vector. The cells were grown to sub-confluence and monolayers were wounded by scraping them with P200 pipette tips, washed to remove cell debris, and refilled with fresh medium. Cells were cultured for 24 hrs and fixed with 4% paraformaldehyde and photographed. (**B**) Diagram of pBABE expression constructs. (**C**) MiR-17-transfected cells were infected with retroviral vector expressing PTEN, GalNT7, or vimentin. The cells were injected into nude mice. Expression of PTEN-, GalNT7- and vimentin were confirmed by immunohistochemistry.

Supplementary Table S1 Age of mice used in the studies and tumor sizes in livers

Mice ID#	Age (days)	Tumor size (mm3)	Tumor/liver ration	Mice ID#	Age (days)	Tumor size (mm3)	Tumor/liver ration
tg5	710	-	-	tg465	134	-	-
tg7	710	-	-	wt466	134	-	-
wt7B	710	-	-	tg469	137	23.05	0.85
wt40	537	-	-	tg470	730	37.3	1.21
tg76	557	-	-	tg475	727	7.05	0.29
tg89	728	10	0.41	tg714	614	4.8	0.28
tg107	707	3.35	0.14	wt718	705	24.9	0.78
wt208	520	-	-	wt726	97	-	-
wt209	520	-	-	wt728	97	-	-
tg230	300	-	-	wt732	39	-	-
wt231	300	-	-	wt748	97	-	-
wt239	291	-	-	tg749	97	-	-
tg240	413	10.12	0.37	wt750	97	-	-
tg244	502	-	-	tg752	97	-	-
tg246	502	-	-	wt753	97	-	-
tg249	502	-	-	wt754	97	-	-
wt256	407	-	-	wt755	97	-	-
wt257	288	-	-	tg787	511	-	-
wt259	407	-	-	tg805	664	10.45	0.40
tg288	386	-	-	tg806	852	-	-
tg290	386	-	-	tg808	664	12.65	0.47
tg291	386	-	-	tg819	372	-	-
wt293	386	-	-	tg848	64	15.4	0.78
wt459	134	-	-	wt862	370	-	-
wt460	134	-	-	tg880	784	-	-
tg461	134	-	-	tg882	676	25	0.85
tg462	134	-	-	tg886	801	6.6	0.27
tg463	134	-	-	tg972	453	17.05	0.78
wt464	134	-	-	tg974	236	-	-

Supplementary Table S2. Primers used in the study

Primer name	Primer sequence
musVIM-R173p-SacI	5’cccggggagctctaaaaattgcacacacttggtgc
musVIM-R173p-MluI	5’gggcccacgcgtctatcttgcgctcctgaaaaactgc
musGalNT7VIM-R17*-SacI	5’cccggggagctctgacaagaacagaggaaaccaacaatc
musGalNT7VIM-R17*-MluI	5’gggcccacgcgtagagcagttttgtaaacagtcactgc
musPten3084-R17-SacI	5’gggagctcagccttaccccgattcagcctcttcag
musPten3084-R17-MluI	5’ccacgcgtttattaagtgatgactaaggct
chver10051-SpeI	5'gggcccactagtaatggagccacatgtatagat
chver10350-SacI	5'gggcccgagctcgaaatcacgctcaaacatctt
human-U6RNAf	5’gtgctcgcttcggcagcacatatac
Human-U6RNAr	5’aaaaatatggaacgcttcacgaatttg
Hu-Gapdh421F	5’aaggctggggctcatttgcag
Hu-Gapdh720R	5’gatgttctggagagccccgcg
EGFP981F	5’caaggacgacggcaactacaagac
EGFPC-ApaI	5’cccgggccccttgtacagctcgtccatgcc